FACETS

FP6-2004-IST-FETPI 15879

Fast Analog Computing with Emergent Transient States

D4-2

Report on conductance based point neurons (with minimal number of ion channels) with parameter sets for 4 prominent neuron types in the FACETS database

Report Version: Final

Report Preparation: A. Destexhe (UNIC)

Classification: Public

Contract Start Date: 01/09/2005 Duration: 4 Years

Project Co-ordinator: Karlheinz Meier (Heidelberg)

Partners: U Bordeaux, CNRS (Gif-sur-Yvette, Marseille), U Debrecen, TU Dresden, U Freiburg, TU Graz, U Heidelberg, EPFL Lausanne, Funetics S.a.r.l., U London, U Plymouth, INRIA, KTH Stockholm

Project funded by the European Community

under the "Information Society Technologies' Programme

DELIVERABLE SUMMARY SHEET

Project Number: FP6-2004-IST-FETPI 15879

Project Acronym: FACETS

Title: Fast Analog Computing with Emergent Transient States

Deliverable N^o: D4-2

Due date: 09-2007

Delivery Date: 09-2007, paper attached Feb. 2009

Short Description:

This deliverable reports on the development of cellular models for cerebral cortex network simulations. The intrinsic electrophysiological properties of cortical neurons were analyzed from several databases and laboratories, and we selected the 4 most prominent electrophysiological classes of neurons. These 4 classes are "fast spiking" (FS), "regular spiking" (RS), "intrinsically bursting" (IB) and "low-threshold spike" (LTS) cells. For each class, we fit the model to experimental data. To obtain models as generic as possible, we used data from different preparations *in vivo* and *in vitro*, such as rat somatosensory cortex, guinea-pig visual cortex, cat visual cortex and cat association cortex. The selection of such cellular models constitutes an important step towards the FACETS model format.

February 2009: Appended the paper "Minimal Hodgkin–Huxley type models for different classes of cortical and thalamic neurons"

Partner owning: UNIC

Partners contributed: UNIC, EPFL

Made available to: Public

Contents

List of Figures

Introduction

This deliverable reports on the development of cellular models for cerebral cortex network simulations. The choice of the type of model was guided by several considerations. Our goal is to represent the "prototypical" types of neurons and synaptic interactions present in neocortex, in order to build large-scale networks. In this report, we focus on models of the intrinsic firing properties of cortical neurons using Hodgkin & Huxley (1952) type models with minimal number of channels. To this aim, we therefore need to (1) capture the main intrinsic firing and response properties of excitatory and inhibitory cortical neurons; (2) if possible capture the diversity of intrinsic properties found in different preparations. These two aspects are detailed below.

The intrinsic electrophysiological properties of cortical neurons are very diverse and were analyzed here from several databases and laboratories. We have used conductance-based spiking neuron models to reproduce a few main neuronal types in neocortex. The electrophysiological classes considered were inspired from the classification of Connors and Gutnick (1990), which was augmented with one additional class. The 4 classes considered are the "fast spiking" (FS), "regular spiking" (RS), "intrinsically bursting" (IB) and "low-threshold spike" (LTS) cells. These classes are reviewed successively in the next sections.

1 Regular spiking neurons

By far the largest cell class in neocortex is the so-called "regular-spiking" (RS) neuron, which is in general excitatory and most often correlates with a spiny pyramidal-cell morphology. The typical response of RS cells to depolarizing current pulses are trains of spikes with adaptation (Fig. 1, *Regular Spiking*).

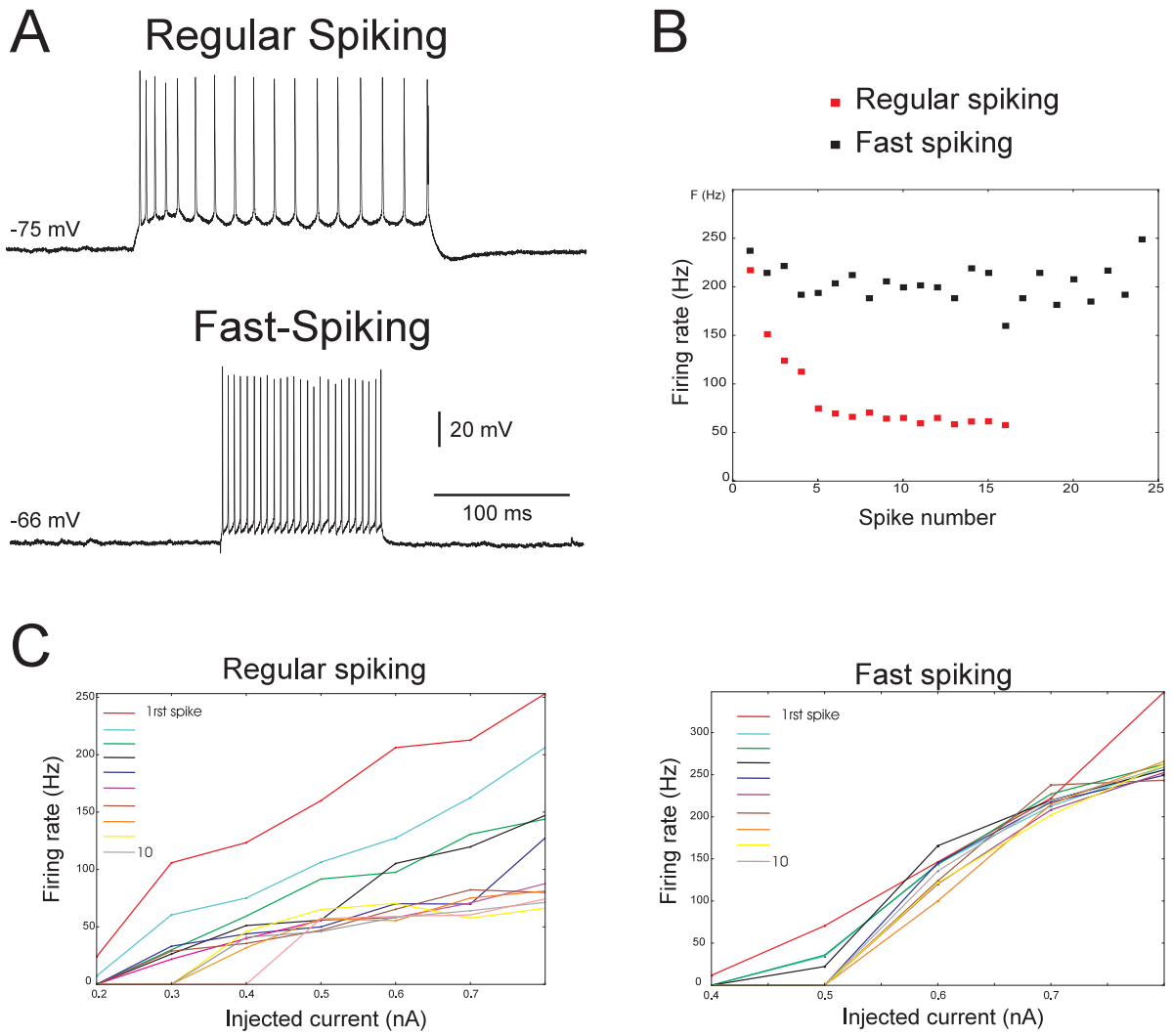

Figure 1. Intracellular recordings of two main classes of neurons in ferret visual cortex *in vitro*. A. Responses to injection of a depolarizing current pulse (0.7 nA). Top: typical response of a regular spiking (RS) neuron, showing spike-frequency adaptation. Bottom: response of a fast-spiking neuron, with negligible adaptation. B. Plot of the instantaneous firing rate (inverse of the interspike interval following the spike) as a function of spike number for these two neurons. C. Frequency-current (F/I) relations for these two neurons. The firing rate was computed as in B and is represented as a function of injected current (amplitude of the pulse). The curves indicated by different colors correspond to first, second, third, ... spikes in the train.

The simplest model of RS cells consists of conductances for generating spikes (I_{Na}, I_{Kd}; kinetics from Traub and Miles, 1990), and in addition, a slow potassium current activated by depolarization, which we call here "I_M" (kinetics from Yamada et al., 1989). This model reproduces the typical firing characteristics of RS cells as recorded in ferret visual cortex *in vitro* (Fig. 2, *Regular Spiking*).

We also realized an automatic fitting of the models to recordings in rat somatosensory cortex *in vitro*. The error function consisted of a weighted sum over the differences in the time of the first spike after DC onset, as well as the first, second and last interspike intervals. Since the data consisted of several trials, the reliability of these criteria could be estimated. The weights were taken to be the inverse of the maximum of either 3% of the respective mean values or the standard deviations. The adjusted parameters were the

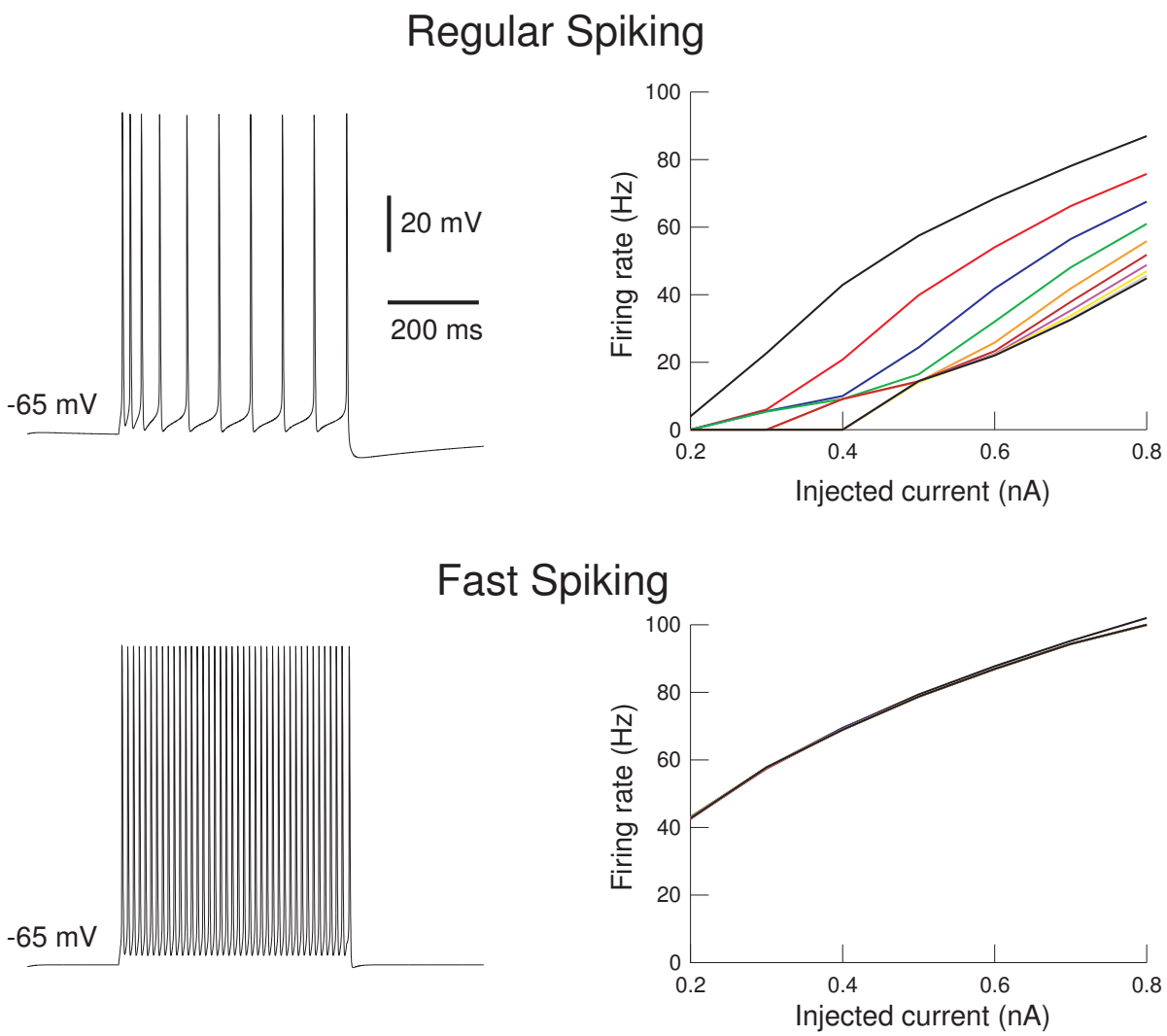

Figure 2. Model of the RS and FS classes of neurons based on ferret visual cortex *in vitro*. Top panels: model of "regular spiking" neuron. The model contained the currents I_{Na} and I_{Kd} responsible for spike generation, with an additional slow K^+ current (I_M) responsible for spike-frequency adaptation. These currents were simulated by Hodgkin-Huxley type models in NEURON. The model exhibited spike frequency adaptation following injection of depolarizing current pulses (left; 0.5 nA injected). The frequency-current (F/I) relation (right) was computed identically as for experiments (Fig. 1C). Bottom panels: same paradigm for a model of "fast spiking" neurons. This model contained only I_{Na} and I_{Kd}. Model parameters (RS): L = d = 96 μm (0.29 nF capacitance), $g_{leak} = 1{\times}10^{-4}$ S/cm^2 (R_{in} of 34.5 MΩ), E_{leak} = -70 mV, $\bar{g}_{Na} = 0.05$ S/cm^2, $\bar{g}_{Kd} = 0.005$ S/cm^2, $\bar{g}_M = 7{\times}10^{-5}$ S/cm^2. Same parameters for FS, except L = d = 67 μm (0.14 nF capacitance), $g_{leak} = 1.5{\times}10^{-4}$ S/cm^2 (R_{in} of 47 MΩ), $\bar{g}_{Kd} = 0.01$ S/cm^2 and no I_M.

leak conductance g_{leak} (bound by $g_{leak}^{phys}/3$ and $3 * g_{leak}^{phys}$, where g_{leak}^{phys} is the leak conductance extracted from experiment), the maximal conductances $\bar{g}_{Na}$ and $\bar{g}_{Kd}$ of the sodium and potassium channels, shifts of their respective activation and inactivation curves (V_T, V_S and V_T') as well as the maximal conductance of I_M and a factor τ_{max} scaling its time constant. We used the simulated annealing fitting algorithm to optimize these parameters. The results of the fitting are shown in Fig. 3 for two RS cells (one pyramidal cell in Fig. 3A, presumed excitatory, and one inhibitory interneuron in Fig. 3B).

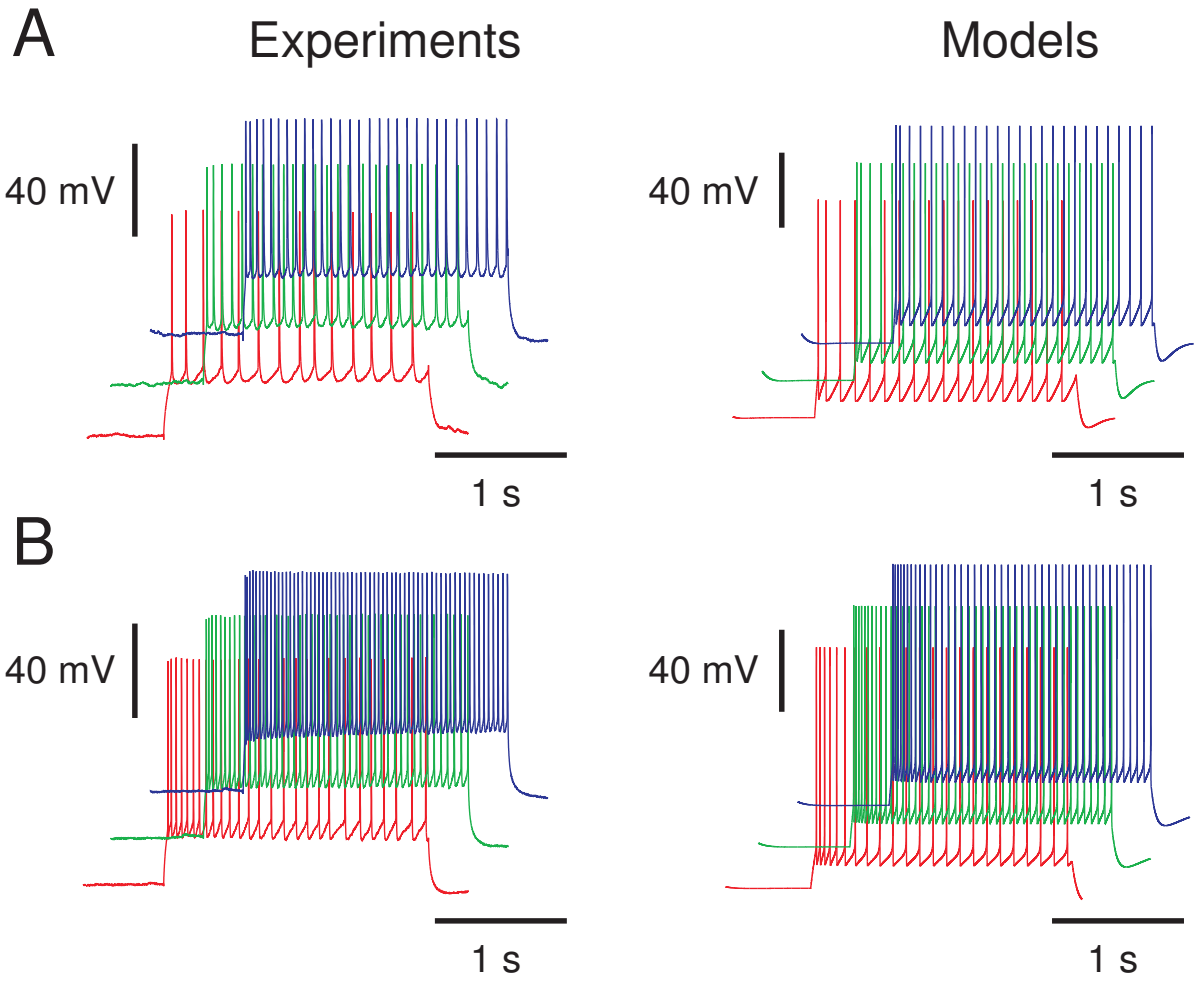

Figure 3. Models of RS neurons based on somatosensory cortex *in vitro*.
Left panels: injection of depolarizing pulses in neurons from rat somatosensory cortex *in vitro*. Right panels: same protocols simulated using the models. A. Regular-spiking pyramidal neuron. Parameters: L = d = 67.6 μm, g_{leak} = 4.17×10^{-5} S/cm^2, E_{leak} = -73.34 mV, $\bar{g}_{Na}$ = 0.022 S/cm^2, V_T = -58.3 mV, V_S = -0.2 mV, $\bar{g}_{Kd}$ = 0.0038 S/cm^2, V'_T = -51.6 mV, $\bar{g}_M$ = 13.1×10^{-5} S/cm^2, τ_{max} = 533 ms. B. Regular-spiking inhibitory neuron. Parameters: L = d = 52.9 μm, g_{leak} = 3.77×10^{-5} S/cm^2, E_{leak} = -62.5 mV, $\bar{g}_{Na}$ = 0.036 S/cm^2, V_T = -59.9 mV, V_S = -1.8 mV, $\bar{g}_{Kd}$ = 0.0024 S/cm^2, V'_T = -60 mV, $\bar{g}_M$ = 1.4×10^{-5} S/cm^2, τ_{max} = 2997 ms. Recordings were from H. Markram's laboratory (http://microcircuit.epfl.ch).

2 Fast spiking neurons

Another major cell class in cerebral cortex is the "fast-spiking" (FS) neuron, which generally corresponds to aspiny inhibitory neurons. FS cells respond to depolarizing pulses by producing high-frequency trains of action potentials with little or no adaptation (Fig. 1, *Fast Spiking*; see also Fig. 4); some interneurons do show adaptation (Fig. 3B). Many other intrinsic firing types have been described for cortical interneurons (Gupta et al., 2000), some of which correspond to RS and FS cells, in addition to classes outlined below.

FS cells are also the simplest type to model, as the conductances for generating spikes (I_{Na}, I_{Kd}) are sufficient. A model based on these two conductances reproduces well the intrinsic firing characteristics of FS cells of ferret visual cortex *in vitro* (Fig. 2, *Fast Spiking*). In some cases, it is necessary to add an adaptation current (I_M) to account for the initial spike-frequency adaptation (Fig. 4).

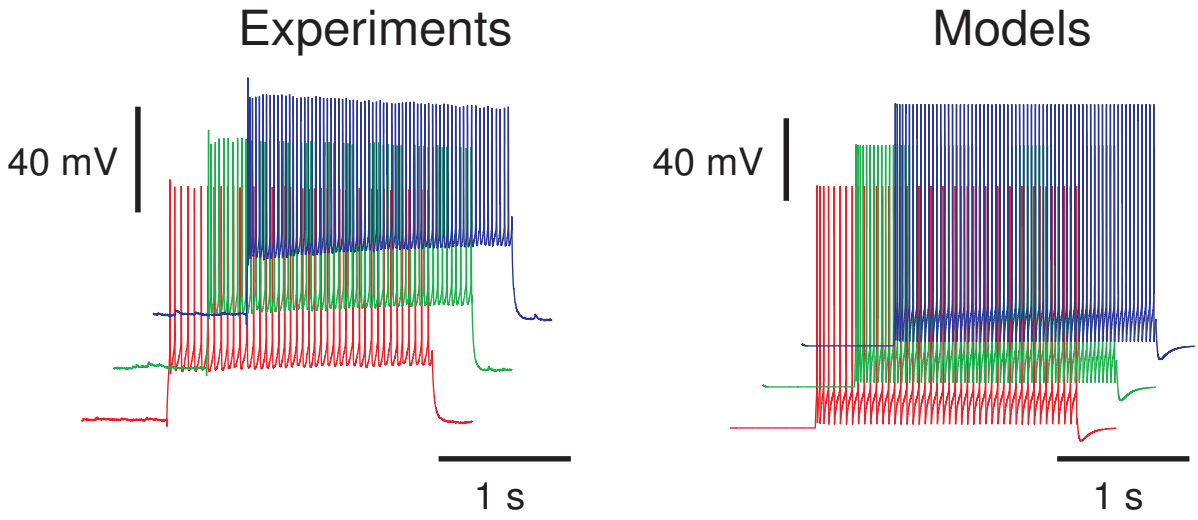

Figure 4. Models of FS neurons based on somatosensory cortex *in vitro*.
Left panels: injection of depolarizing pulses in a FS neuron from rat somatosensory cortex *in vitro*. Right panels: same protocols simulated using the models. Parameters: L = d = 56.9 μm, g_{leak} = 6.44×10^{-5} S/cm^2, E_{leak} = -70.2 mV, $\bar{g}_{Na}$ = 0.039 S/cm^2, V_T = -59.9 mV, V_S = -0.8 mV, $\bar{g}_{Kd}$ = 0.0061 S/cm^2, V'_T = -53.3 mV, $\bar{g}_M$ = 7.7×10^{-5} S/cm^2, τ_{max} = 510 ms. Recordings were from H. Markram's laboratory (http://microcircuit.epfl.ch).

3 Intrinsically bursting neurons

Another very common cell class is the "intrinsically bursting" (IB) neuron. This type of neuron generates bursts of action potentials following depolarizing stimuli, and represents a few percent of the recorded cells in primary sensory cortex, both *in vivo* and *in vitro*. Fig. 5A shows a bursting cell recorded in guinea pig somatosensory cortex *in vitro* (from McCormick et al., 1985) and Fig. 6A shows a bursting cell recorded in cat primary visual cortex *in vivo*. When submitted to depolarizing current pulses, IB cells first generate a burst of action potentials followed by single spikes with adaptation. This behavior is typical of IB neocortical neurons (Connors and Gutnick, 1990).

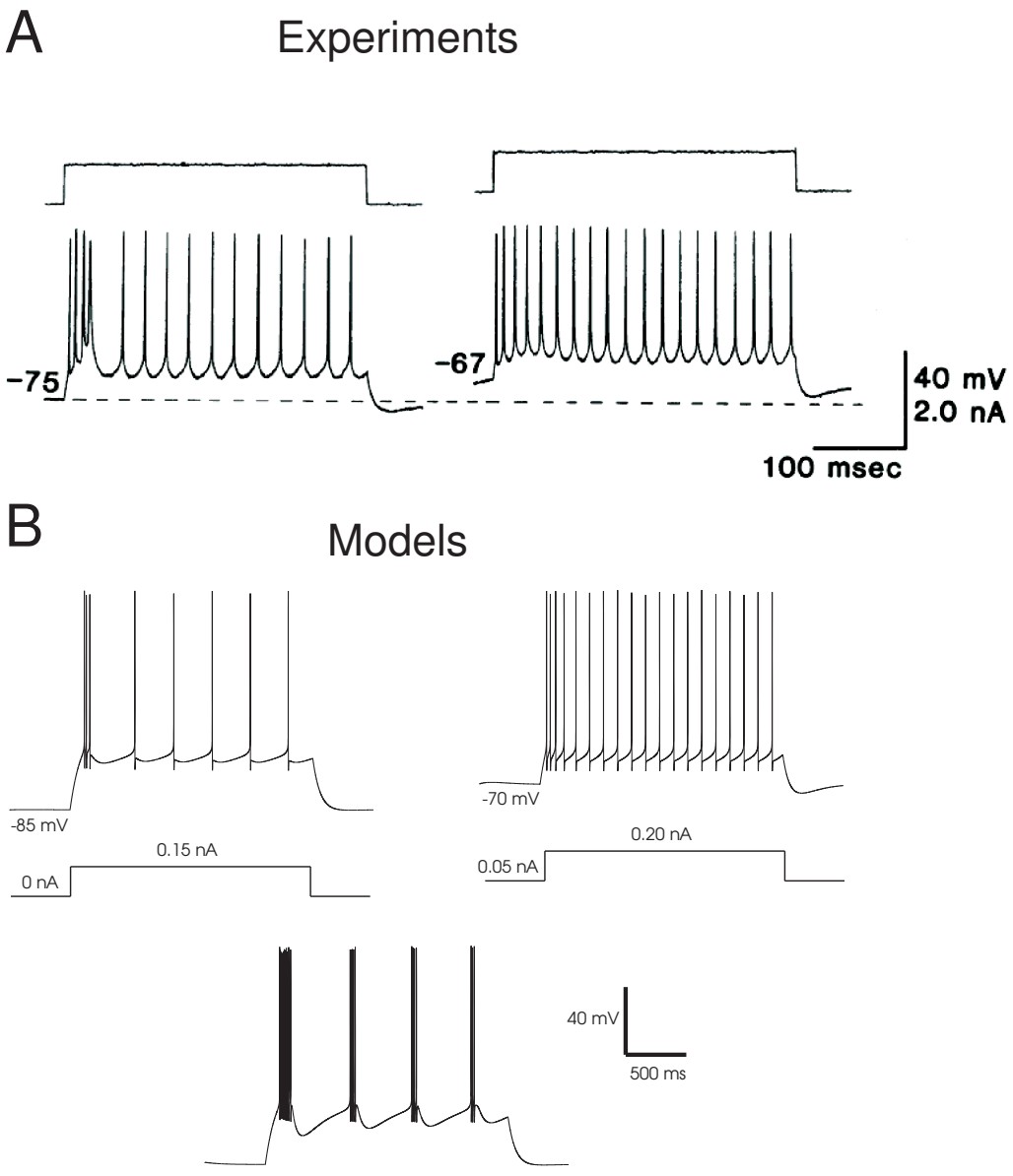

Figure 5. Model of intrinsically bursting cell based on guinea-pig somatosensory cortex *in vitro*. The model consisted of a RS cell augmented with the L-type calcium current I_L, thus comprising I_{Na}, I_K, I_M and I_L currents. A. Intrinsically bursting (IB) cell from guinea-pig somatosensory cortex *in vitro* (modified from McCormick et al., 1985). The response to the same depolarizing current pulse is shown at two different DC levels. B. Response to depolarizing current in a model of IB cell. Top panels: similar protocol as in A; Bottom panel: repetitive bursting activity with larger L-type conductance. Parameters: L = d = 96 μm (0.29 nF capacitance), g_{leak} = 1×10^{-5} S/cm^2, E_{leak} = -70 mV, $\bar{g}_{Na}$ = 0.05 S/cm^2, $\bar{g}_{Kd}$ = 0.005 S/cm^2, $\bar{g}_M$ = 3×10^{-5} S/cm^2, $\bar{g}_L$ = 0.0001 S/cm^2 (0.0002 S/cm^2 for the bottom panel).

We modeled IB cells based on a minimal set of channels. To generate the bursting behavior, we

extended the previous model of RS cell by adding the L-type calcium current (kinetics from the model of Reuveni et al., 1993, based on experiments described in Sayer et al., 1990). In a first set of models, we generated IB type behavior by using moderate densities of I_L, and compared the behavior of the model with data obtained in the sensorimotor cortex of guinea pigs (Fig. 5A). This model generated an initial burst followed by an adapting train of action potentials (Fig. 5B, top). With larger L-type conductance, this model generated repetitive bursting activity (Fig. 5B, bottom).

We also adjusted this model to data from cat primary visual cortex *in vivo* (Fig. 6A). The density of I_L was adjusted to match the response to depolarizing current pulses (Fig. 6B). As above, if depolarizing pulses were given from hyperpolarized levels, this model generated an initial burst followed by an adapting train of action potentials (Fig. 6B).

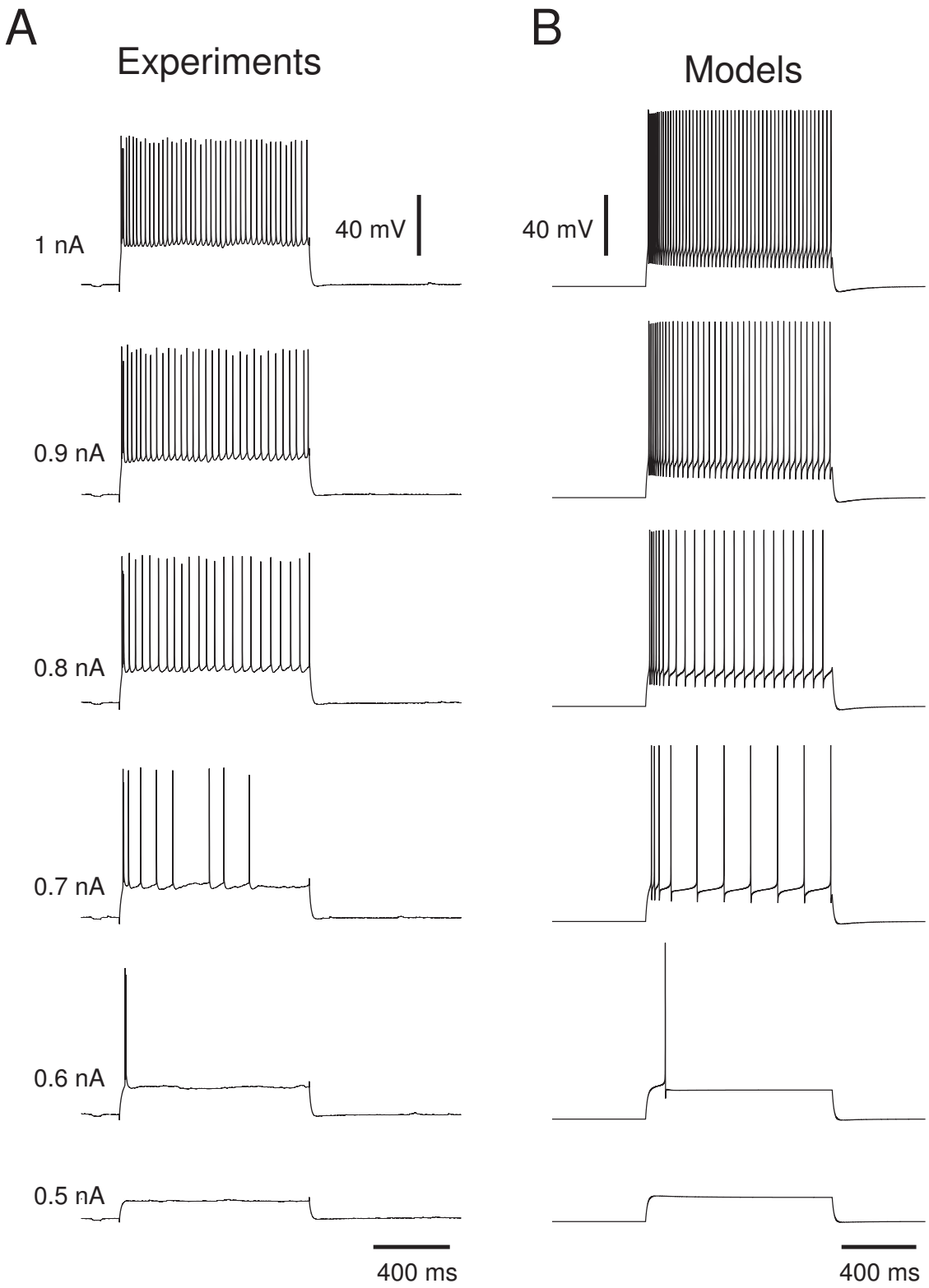

Figure 6. Model of intrinsically bursting cell based on cat visual cortex neurons *in vivo.* The model consisted of a RS cell augmented with the L-type calcium current I_L, thus comprising I_{Na}, I_K, I_M and I_L currents. A. Intrinsically bursting (IB) cell from cat primary visual cortex in vivo. Responses to depolarizing current pulses are shown from top to bottom. Values of the injected current were from 0.5 to 1 nA as indicated. B. Same protocol simulated using the model. The parameters were: L = d = 96 μm (0.29 nF capacitance), g_{leak} = 1×10^{-4} S/cm^2 (R_{in} of 34.5 MΩ), E_{leak} = -75 mV, $\bar{g}_{Na}$ = 0.05 S/cm^2, V_T = -58 mV, $\bar{g}_{Kd}$ = 0.0042 S/cm^2, $\bar{g}_M$ = 4.2×10^{-5} S/cm^2, τ_{max} = 1000 ms, $\bar{g}_L$ = 0.00012 S/cm^2. Recordings were from Y. Frégnac's laboratory (http://www.unic.cnrs-gif.fr).

4 Low-threshold spiking neurons

In a previous study (Destexhe et al., 2001), we observed low-threshold spike (LTS) activity in a significant fraction (about 10%) of intracellularly-recorded cells in cat association cortex *in vivo* (Fig. 7A). These LTS neurons generated adapting trains of action potentials in response to depolarizing current injection (Fig. 7A, left panel), similar to the classic "regular-spiking" response of cortical neurons. In addition, they generated a burst of action potentials in response to injection of hyperpolarizing current pulses (Fig. 7A, right panel). This property was also identified in deep layers of guinea-pig cerebral cortex *in vitro* (de la Peña and Geijo-Barrientos, 1996; see Fig. 7B) and was shown to be due to the presence of the T-type (low-threshold) calcium current I_T.

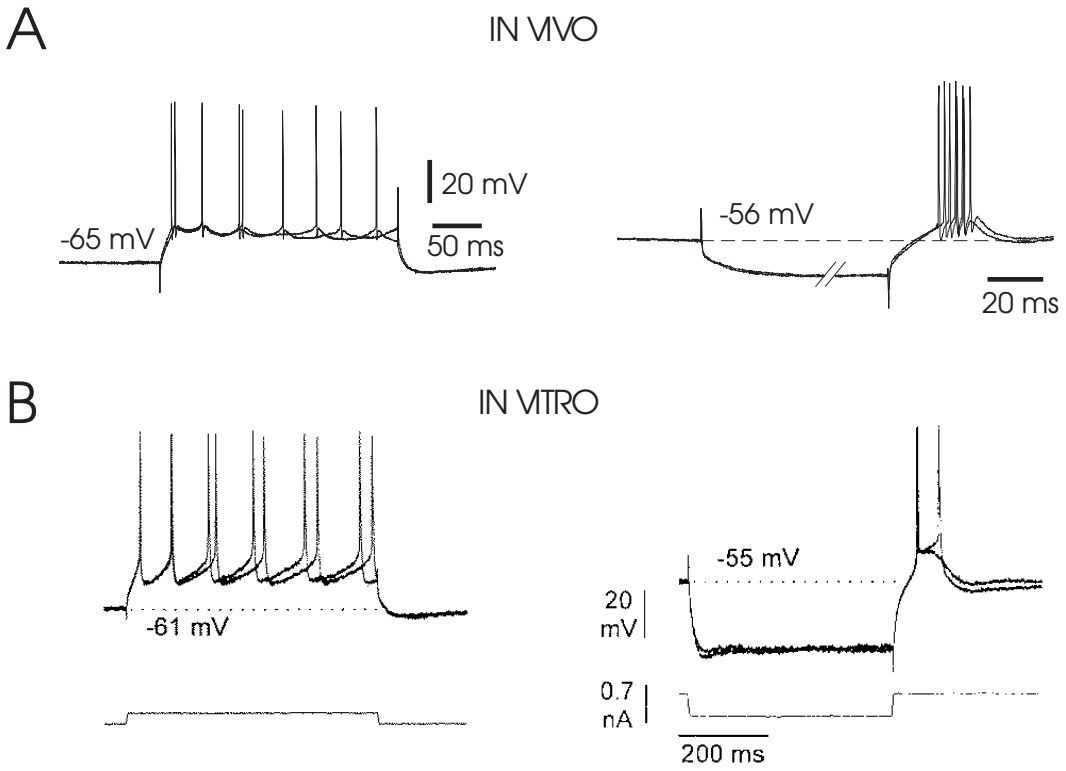

Figure 7. Rebound bursting properties of cortical pyramidal cells of cat association cortex *in vivo*. A. Rebound bursting cell from cat cerebral cortex *in vivo* (from Destexhe et al., 2001). B. Rebound bursting cell from guinea-pig frontal cortex *in vitro* (adapted from de la Peña and Geijo-Barrientos, 1996). In both cases, the response to depolarizing current pulses was similar to a regular spiking cell. In addition, LTS cells produce a burst of action potentials in rebound to hyperpolarizing current pulses (-0.1 nA; the pulse was 200 ms in A and was truncated for clarity).

We have attempted to model these intrinsic firing properties based on a minimal set of channels. To generate rebound bursting behavior, the T-type calcium current was included (kinetics from Destexhe et al., 1996) and its peak amplitude was adjusted to match voltage-clamp recordings of this current in pyramidal neurons (de la Peña and Geijo-Barrientos, 1996). A density of T-channels of 0.8 mS/cm^2 was needed to match the relatively small amplitude of this current measured in pyramidal neurons. Using this density, the model could generate weak rebound bursts at the offset of hyperpolarizing current (Fig. 8A, -60 mV). To generate the classic "regular-spiking" behavior (Fig. 8B, -70 mV), the model included three voltage-dependent currents identical to above for RS cells: a slow voltage-dependent K^+ current (I_M), as I_{Na} and I_{Kd} currents for action potential generation. If depolarizing pulses were given from hyperpolarized levels, this model generated an initial burst followed by an adapting train of action potentials (Fig. 8C, -80 mV), which is a feature often observed in neocortical neurons (Connors and Gutnick, 1990).

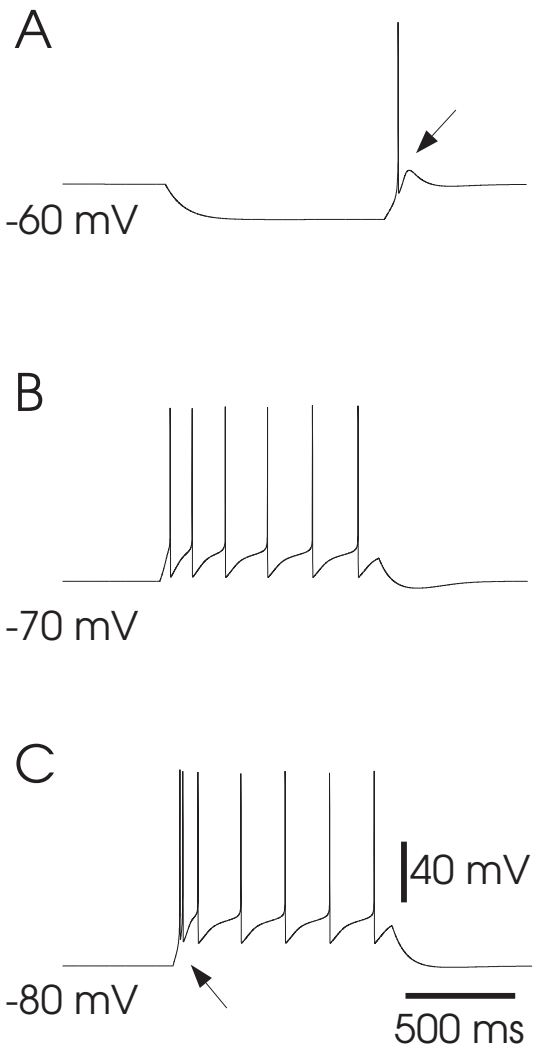

Figure 8. Model of rebound bursting cell of cat association cortex *in vivo*.
The model consisted of a RS cell augmented with the T-type calcium current I_T, thus comprising I_{Na}, I_K, I_M and I_T currents. A. Rebound burst response at the offset of a hyperpolarizing current pulse (-0.1 nA). B. Adapting train of action potentials with depolarizing current pulses. C. Similar depolarizing pulse showing a burst of action potentials followed by single spikes. Arrows indicate bursts of action potentials mediated by I_T. Model parameters: L = d = 96 μm (0.29 nF capacitance), $g_{leak} = 1\times10^{-5}$ S/cm^2, E_{leak} = -85 mV, $\bar{g}_{Na}$ = 0.05 S/cm^2, $\bar{g}_{Kd}$ = 0.005 S/cm^2, $\bar{g}_M = 3\times10^{-5}$ S/cm^2, $\bar{g}_T$ = 0.0004 S/cm^2. Figure modified from Destexhe et al., 2001.

In addition, we also considered LTS cells from rat somatosensory cortex *in vitro* (Fig. 9, *Experiments*). As seen above, this LTS cell generated adapting trains of action potentials in response to depolarizing pulses (Fig. 9A, *Experiments*), as well as rebound burst activity at the offset of hyperpolarizing current pulses (Fig. 9B, *Experiments*). We used the same model as above, but changed the parameters such that it matches the input resistance of this LTS neuron (which was 210 MΩ for this particular cell), and approximates at best the frequency/current relationship of the cell (not shown). The resulting model is shown in Fig. 9A-B (*Models*) for the exact same protocol as for the experiments.

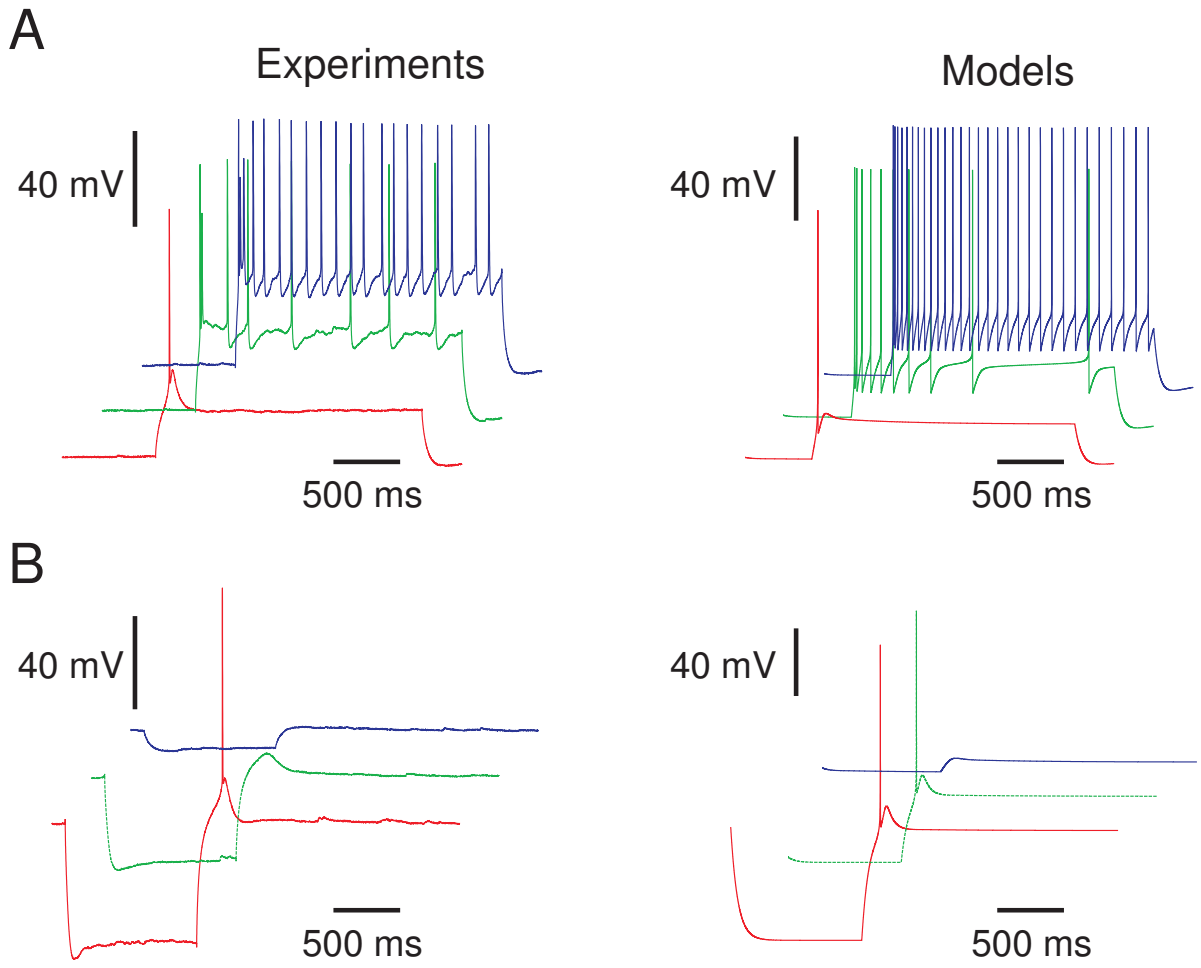

Figure 9. Model of rebound bursting cell based on rat somatosensory cortex *in vitro*.
The model had the same current as the "cat" model, but different parameters. A. LTS cell from rat somatosensory cortex in vitro. The top panel shows the response to depolarizing current pulses, while the response to hyperpolarizing pulses is shown in the bottom panel. Values of the injected current were: -0.015, 0.067 and 0.13 nA for depolarizing pulses (DC current was -0.11 nA to bring the cell to -70 mV; they were of -0.36, -0.24 and -0.09 nA for hyperpolarizing pulses (pre-pulse current of -0.056 nA to bring the cell to -60 mV. B. Same protocols simulated using the model. The parameters were: L = d = 89.2 μm (0.25 nF capacitance), g_{leak} = 1.9×10^{-5} S/cm^2, E_{leak} = -50 mV, $\bar{g}_{Na}$ = 0.05 S/cm^2, V_T = -50 mV, $\bar{g}_{Kd}$ = 0.004 S/cm^2, $\bar{g}_M$ = 2.8×10^{-5} S/cm^2, $\bar{g}_T$ = 0.0004 S/cm^2, V_x = -7 mV.

5 Thalamic relay neurons

It is important to note that the model of LTS cell is very similar to models for thalamic relay cells. There are, however, two notable differences. First, thalamic relay cells do not show spike-frequency adaptation, so no adaptation current, such as I_M, is needed. Second, the thalamic relay cell produces more powerful bursts compared to cortical LTS cells, presumably because the T-type calcium current I_T has a larger conductance in thalamic cells. In voltage-clamp experiments, the peak amplitude of I_T in pyramidal neurons of guinea-pig cerebral cortex is of about 0.4-0.8 nA (de la Peña and Geijo-Barrientos, 1996), which is small compared to the peak amplitude of I_T in thalamic relay cells (5.8 $\pm$ 1.7 nA in Destexhe et al., 1998). Figure 10 shows models of thalamic relay cell obtained previously. Current-clamp (Fig. 10A) and voltage-clamp (Fig. 10C) recordings were used to adjust the model. A detailed model based on morphological reconstructions was first obtained (Fig. 10B). This model was then simplified into a single-compartment model comprising I_T, I_{Na} and I_{Kd} currents (Fig. 10D; same kinetics as above; see details in Destexhe et al., 1998).

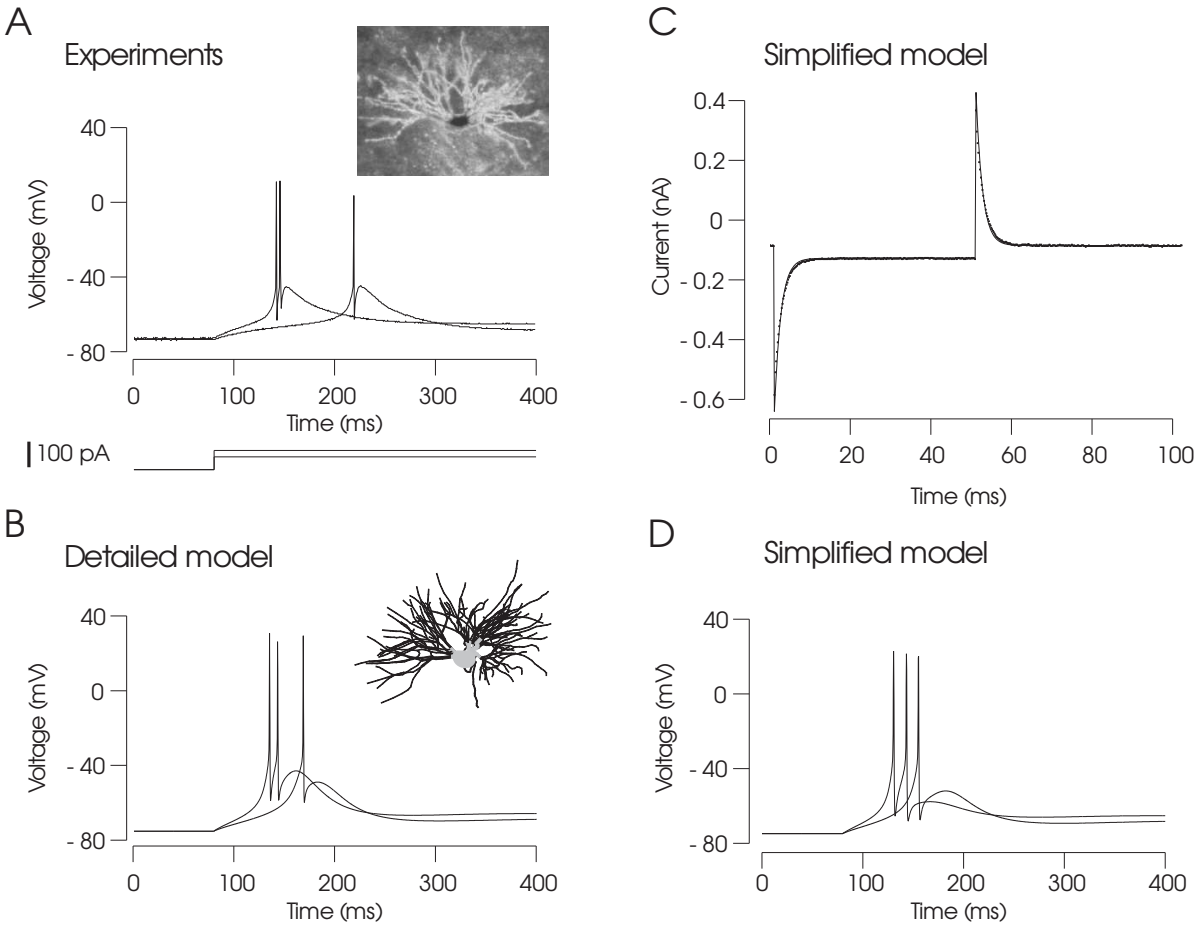

Figure 10. Model of thalamic relay neuron from rat somatosensory thalamus *in vitro*.
A. Current-clamp recordings of a relay cell from the ventrobasal thalamus (inset), subjected to depolarizing current pulses. The cell produced a rebound burst of action potentials. B. Detailed model based on the morphology of the recorded cell (which was reconstructed and incorporated into simulations). The inset shows the reconstructed cell model (soma in gray). C. Adjustment of a one-compartment model to passive responses recorded in voltage-clamp in the cell shown in A (dots; model showed as a continuous trace). D. Current-clamp simulation of the same protocol as in A. Modified from Destexhe et al., 1998 where all details were given.

6 Conclusion

In this report, we have summarized modeling efforts within FACETS to select a few electrophysiological cell classes. The aim of this approach is to obtain a model format that can account for the diversity of cell intrinsic properties in cerebral cortex, both for excitatory and inhibitory neurons. This constitutes an important step towards obtaining a common FACETS model format for network simulations.

We have selected four cell classes, the "fast spiking" (FS), "regular spiking" (RS), "intrinsically bursting" (IB) and "low-threshold spike" (LTS) cells. For each cell class, we have analyzed intracellular recordings from different preparations (when possible) and obtained models for each cell class. In some cases, the models were adjusted using automatic fitting procedures.

The models considered here are the simplest types of biophysical models where the intrinsic properties arise from voltage-dependent conductances, each described by differential equations (Hodgkin-Huxley type models). Such models are implementable on the VLSI hardware, and some of these models (RS and FS cells) have already been implemented by S. Renaud and colleagues at the ENSEIRB (Zou et al., 2006). Another motivation is to build biophysically semi-realistic network models of cerebral cortex which incorporate the diversity of intrinsic cell properties in cortex.

Two important points must be noted. First, the choice of a specific cell class is not restricted to excitatory or inhibitory neurons. Any cell class can be used for any cell type, for instance LTS, IB and RS type of properties have been found for both excitatory or inhibitory neurons in cortex. In addition, the LTS cell class can be used to model thalamic neurons. Second, we described here four distinct cell properties, but in general the properties are not so clear-cut. It is important to note that these models can be changed at will to diversify the neuron types. For example, the time constant τ_{max} of the adaptation current I_M can be adjusted to yield fast or slow adaptation. From our fitting to spike-frequency adaptation, the values of τ_{max} range from a few hundred of milliseconds to several seconds.

The next step is now to design simpler representations of cellular models based on the integrate-and-fire model. For instance, the Izhikevich type of models are two-variable extensions of the integrate-and-fire model and they can capture the diversity of firing patterns in cortical neurons (Izhikevich, 2004). This model was extended later to obtain more realistic approach of the V_m to spike threshold (Brette and Gerstner, 2005). The latter model is also easier to fit to experimental data (cfr W. Gerstner and colleagues at EPFL) and is therefore more adequate to be fitted to experimental data within FACETS. This model was chosen to be implemented on VLSI hardware by K. Meier and colleagues at UHEI. Obtaining similar cell classes as obtained here, but using the Brette-Gerstner model, constitutes the next step towards the FACETS model format.

Appendix: Equations of the models

Membrane equation

All models described here were single-compartment neurons (cylinder of diameter d and length L) described by the following membrane equation:

$$C_m \frac{dV}{dt} = -g_{leak}(V - E_{leak}) - I_{Na} - I_{Kd} - I_M - I_T - I_L \ , \tag{1}$$

where V is the membrane potential, $C_m = 1\mu F/cm^2$ is the specific capacitance of the membrane, g_{leak} is the resting (leak) membrane conductance, E_{leak} is its reversal potential. I_{Na} and I_{Kd} are the sodium and potassium currents responsible for action potentials, I_M is a slow voltage-dependent potassium current responsible for spike-frequency adaptation, I_L is a high-threshold calcium current and I_T is a low-threshold calcium current. These voltage-dependent currents are variants of the same generic equation:

$$I_j = \bar{g}_j \ m^M h^N \ (V - E_j) \ , \tag{2}$$

where the current I_j is expressed as the product of respectively the maximal conductance, $\bar{g}_j$, activation (m) and inactivation variables (h), and the difference between the membrane potential V and the reversal potential E_j. The gating of the channel is derived from the following first order kinetic scheme:

$$C \underset{\beta(V)}{\overset{\alpha(V)}{\rightleftharpoons}} O \tag{3}$$

where O and C are the open and closed states of the gate. The variables m and h represent the fraction of independent gates in the open state, following the convention introduced by Hodgkin and Huxley (1952). The steady-state activation and the time constant are, respectively, given by $m_\infty = \alpha/(\alpha + \beta)$ and $\tau_m = 1/(\alpha + \beta)$, and similarly for h.

Details for each voltage-dependent current

All kinetics below correspond to a temperature of $36\,^\circ C$.

Sodium and potassium currents to generate action potentials

The voltage-dependent Na^+ current was described by a modified version of Hodgkin-Huxley equations adapted for central neurons (Traub and Miles, 1991), which is particularly well suited for hippocampal and cortical pyramidal cells:

$$\begin{aligned}
I_{Na} &= \bar{g}_{Na} \ m^3 h \ (V - E_{Na}) \\
\frac{dm}{dt} &= \alpha_m(V) \ (1 - m) \ - \ \beta_m(V) \ m \\
\frac{dh}{dt} &= \alpha_h(V) \ (1 - h) \ - \ \beta_h(V) \ h \\
\alpha_m &= \frac{-0.32 \ (V - V_T - 13)}{\exp[-(V - V_T - 13)/4] - 1} \\
\beta_m &= \frac{0.28 \ (V - V_T - 40)}{\exp[(V - V_T - 40)/5] - 1} \\
\alpha_h &= 0.128 \ \exp[-(V - V_T - V_S - 17)/18] \\
\beta_h &= \frac{4}{1 + \exp[-(V - V_T - V_S - 40)/5]} \ .
\end{aligned} \tag{4}$$

Unless stated otherwise, $\bar{g}_{Na} = 50$ mS/cm^2 and $E_{Na} = 50mV$. V_T adjusts spike threshold and V_S shifts inactivation with respect to activation.

The "delayed-rectifier" K^+ current was described by (Traub and Miles, 1991):

$$\begin{aligned} I_{Kd} &= \bar{g}_{Kd}\, n^4\, (V - E_K) \\ \frac{dn}{dt} &= \alpha_n(V)\, (1 - n) \; - \; \beta_n(V)\, n \\ \alpha_n &= \frac{-0.032\, (V - V'_T - 15)}{\exp[-(V - V'_T - 15)/5] - 1} \\ \beta_n &= 0.5\, \exp[-(V - V'_T - 10)/40] \;, \end{aligned}$$

where $\bar{g}_{Kd} = 5$ mS/cm^2 and $E_K = -90mV$, unless stated otherwise.

Slow potassium current for spike-frequency adaptation

A slow noninactivating K^+ current was described by (Yamada et al., 1989):

$$\begin{aligned} I_M &= \bar{g}_M\, p\, (V - E_K) \\ \frac{dp}{dt} &= (p_\infty(V) - p)/\tau_p(V) \\ p_\infty(V) &= \frac{1}{1 + \exp[-(V + 35)/10]} \\ \tau_p(V) &= \frac{\tau_{max}}{3.3\, \exp[(V + 35)/20] + \exp[-(V + 35)/20]} \;, \end{aligned}$$

where $\bar{g}_M$ was 0.004 mS/cm^2 and $\tau_{max} = 4$ s, unless stated otherwise.

Calcium currents to generate bursting

A first type of bursting was modeled by the high-threshold Ca^{2+} current, which was described by (Reuveni et al., 1993):

$$\begin{aligned} I_L &= \bar{g}_L\, q^2 r (V - E_{Ca}) \\ \frac{dq}{dt} &= \alpha_q(V)\, (1 - q) \; - \; \beta_q(V)\, q \\ \frac{dr}{dt} &= \alpha_r(V)\, (1 - r) \; - \; \beta_r(V)\, r \\ \alpha_q &= \frac{0.055\, (-27 - V)}{\exp[(-27 - V)/3.8] - 1} \\ \beta_q &= 0.94\, \exp[(-75 - V)/17] \\ \alpha_r &= 0.000457\, \exp[(-13 - V)/50] \\ \beta_r &= \frac{0.0065}{exp[(-15 - V)/28] + 1} \;, \end{aligned}$$

where $\bar{g}_L$ is the maximum conductance of the I_L current, and the reversal potential for Ca^{2+} ions was $E_{Ca} = 120$ mV.

A second type of bursting (rebound bursts) was modeled by the low-threshold Ca^{2+} current, which was initially designed for thalamic neurons (Destexhe et al., 1996; see Huguenard and McCormick, 1992

for voltage-clamp data), and is given by:

$$\begin{aligned} I_T &= \bar{g}_T \; s_\infty^2 u \; (V - E_{Ca}) \\ \frac{du}{dt} &= (u_\infty(V) - u)/\tau_u(V) \\ s_\infty(V) &= \frac{1}{1 + \exp[-(V + V_x + 57)/6.2]} \\ u_\infty(V) &= \frac{1}{1 + \exp[(V + V_x + 81)/4]} \\ \tau_s(V) &= \frac{30.8 + (211.4 + \exp[(V + V_x + 113.2)/5])}{3.7 \; (1 + \exp[(V + V_x + 84)/3.2)]}) \; , \end{aligned}$$

where $\bar{g}_T$ is the maximal conductance of the T-current and $V_x = 2$ mV is a uniform shift of the voltage dependence. Note that the activation variable s is considered here at steady-state, because the activation in fast compared to inactivation. This T-current model was also used with an independent activation variable (Destexhe et al., 1998; Fig. 10), but produced very similar results as the model with activation at steady-state (not shown).

References

Brette, R., and Gerstner, W. Adaptive exponential integrate-and-fire model as an effective description of neuronal activity. J. Neurophysiol. 94: 3637-3642, 2005.

Connors, B.W. and Gutnick, M.J. Intrinsic Firing patterns of diverse neocortical neurons. Trends Neurosci. 13: 99-104, 1990.

de la Peña E and Geijo-Barrientos E. Laminar organization, morphology and physiological properties of pyramidal neurons that have the low-threshold calcium current in the guinea-pig frontal cortex. J. Neurosci. 16: 5301-5311, 1996.

Destexhe, A., Bal, T., McCormick, D.A. and Sejnowski, T.J. Ionic mechanisms underlying synchronized oscillations and propagating waves in a model of ferret thalamic slices. J. Neurophysiol. 76: 2049-2070, 1996.

Destexhe, A. Contreras, D. and Steriade, M. LTS cells in cerebral cortex and their role in generating spike-and-wave oscillations. Neurocomputing 38: 555-563, 2001.

Destexhe, A., Neubig, M., Ulrich, D. and Huguenard, J.R. Dendritic low-threshold calcium currents in thalamic relay cells. J. Neurosci. 18: 3574-3588, 1998.

Gupta, A., Wang, Y. and Markram, H. Organizing principles for a diversity of GABAergic interneurons and synapses in the neocortex. Science 287: 273-278, 2000.

Hines, M.L. and Carnevale, N.T., The Neuron simulation environment. Neural Computation 9: 1179-1209, 1997.

Hodgkin, A.L. and Huxley, A.F. A quantitative description of membrane current and its application to conduction and excitation in nerve. J. Physiol. 117: 500-544, 1952.

Huguenard, J.R. and McCormick, D.A. Simulation of the currents involved in rhythmic oscillations in thalamic relay neurons. J. Neurophysiol. 68: 1373-1383, 1992.

Izhikevich, E.M. Which model to use for cortical spiking neurons? IEEE Trans. Neural Networks. 15: 1063-1070, 2004.

McCormick, D.A., Connors, B.W., Lighthall, J.W. and Prince, D.A. Comparative electrophysiology of pyramidal and sparsely spiny stellate neurons of the neocortex. J. Neurophysiol. 54: 782-806, 1985.

Reuveni I, Friedman A, Amitai Y and Gutnick MJ. Stepwise repolarization from Ca^{2+} plateaus in neocortical pyramidal cells: evidence for nonhomogeneous distribution of HVA Ca^{2+} channels in dendrites. J. Neurosci. 13: 4609-4621, 1993.

Sayer RJ, Schwindt PC and Crill WE. High- and low-threshold calcium currents in neurons acutely isolated from rat sensorimotor cortex. Neurosci. Letters 120: 175-178, 1990.

Traub, R.D. and Miles, R. *Neuronal Networks of the Hippocampus.* Cambridge University Press, Cambridge UK, 1991.

Yamada, W.M., Koch, C. and Adams, P.R. Multiple channels and calcium dynamics. In: *Methods in Neuronal Modeling*, edited by C. Koch and I. Segev, MIT press, Cambridge MA, 1989, pp. 97-134.

Zou, Q., Bornat, Y., Saïghi, S., Tomas, J., Renaud, S. and Destexhe, A. Analog-digital simulations of full conductance-based networks of spiking neurons with spike timing dependent plasticity. Network 17: 211-233, 2006.

Biol Cybern (2008) 99:427–441
DOI 10.1007/s00422-008-0263-8

PROSPECTS

Biological Cybernetics

Minimal Hodgkin–Huxley type models for different classes of cortical and thalamic neurons

Martin Pospischil · Maria Toledo-Rodriguez · Cyril Monier · Zuzanna Piwkowska · Thierry Bal · Yves Frégnac · Henry Markram · Alain Destexhe

Received: 4 February 2008 / Accepted: 16 September 2008

Abstract We review here the development of Hodgkin–Huxley (HH) type models of cerebral cortex and thalamic neurons for network simulations. The intrinsic electrophysiological properties of cortical neurons were analyzed from several preparations, and we selected the four most prominent electrophysiological classes of neurons. These four classes are "fast spiking", "regular spiking", "intrinsically bursting" and "low-threshold spike" cells. For each class, we fit "minimal" HH type models to experimental data. The models contain the minimal set of voltage-dependent currents to account for the data. To obtain models as generic as possible, we used data from different preparations in vivo and in vitro, such as rat somatosensory cortex and thalamus, guinea-pig visual and frontal cortex, ferret visual cortex, cat visual cortex and cat association cortex. For two cell classes, we used automatic fitting procedures applied to several cells, which revealed substantial cell-to-cell variability within each class. The selection of such cellular models constitutes a necessary step towards building network simulations of the thalamocortical system with realistic cellular dynamical properties.

M. Pospischil · C. Monier · Z. Piwkowska · T. Bal · Y. Frégnac · A. Destexhe
Unité de Neurosciences Intégratives et Computationnelles (UNIC), CNRS, Gif-sur-Yvette, France

M. Toledo-Rodriguez
Brain and Body Centre, University of Nottingham, Nottingham, UK

H. Markram
Brain and Mind Institute, EPFL, Lausanne, Switzerland

A. Destexhe (✉)
UNIC, Bat 33, CNRS, 1 Avenue de la Terrasse, 91198 Gif-sur-Yvette, France
e-mail: Destexhe@unic.cnrs-gif.fr; destexhe@iaf.cnrs-gif.fr

Keywords Computational models · Cerebral cortex · Thalamus · Intrinsic neuronal properties · Biophysical models · Model fitting · Intracellular recordings

1 Introduction

Central neurons are characterized by a wide diversity of intrinsic cellular properties (reviewed in Llinás 1988; Connors and Gutnick 1990; Gupta et al. 2000). To design network models of the thalamocortical system which take into account this diversity, one needs to obtain precise single-cell models that capture these intrinsic properties. In particular, for large-scale networks, it is necessary to have models that are not only dynamically precise, but also fast and efficient to simulate. Candidates for such "simplified" models, are either integrate-and-fire models, in particular those who can capture complex firing properties (Smith et al. 2000; Izhikevich 2004; Brette and Gerstner 2005), or Hodgkin and Huxley (1952) type models. In the present paper, we focus on the latter type to model the intrinsic properties of thalamic and cortical neurons.

To estimate the parameters of models, automatic fitting procedures were used since over a decade, starting from detailed compartmental models with full dendritic morphology (Destexhe et al. 1996a, b, 1998; Eichler-West and Wilcox 1997; Baldi et al. 1998; Achard and De Schutter 2006; Druckmann et al. 2007). Although this approach provides estimates of the conductance densities, it was shown that different parameter sets can give the same output (Bhalla and Bower 1993; Marder et al. 2007), and that generally, the relationship between model output and the values of the parameters is often very complex (Foster et al. 1993; Golowasch et al. 2002; Achard and De Schutter 2006; Taylor et al. 2006). It was suggested that for such models, more meaningful and

robust estimates are obtained if one uses the morphology and recordings from the same cell (Holmes et al. 2006). Examples of fitting morphologically-reconstructed model cells to the recordings from the same cell are available for different types of neurons (Cauller and Connors 1992; Rall et al. 1992; Stratford et al. 1989; Major et al. 1994; Rapp et al. 1994; Destexhe et al. 1998; Stuart and Spruston 1998).

Automatic fitting procedures were applied later to single-compartment models, such as Hodgkin and Huxley (1952) type models (Foster et al. 1993; Tawfik and Durand 1994; Haufler et al. 2007), as well as integrate-and-fire type models (Rauch et al. 2003; Jolivet et al. 2004). In these cases, a more exhaustive parameter space exploration is possible because these models are much faster to simulate compared to compartmental models. It was also shown that a critical aspect is the error function chosen to evaluate the performance of a given model (Rall et al. 1992; LeMasson and Maex 2001; see also Tien and Guckenheimer 2008 for bursting models). There exists at present no consensus on how to choose the error function, except that simple functions such as the mean square error between the model and experimental membrane potentials is dangerous, because it is highly sensitive to the exact spike shape and timing. Measures defined on distance in phase space (LeMasson and Maex 2001) or based on qualitative features such as action potential amplitude and width (Druckmann et al. 2007) are preferable and give models close to the "hand-fitted" models used traditionally. We will follow here a similar approach and use error functions based on qualitative features of the membrane potential (V_m) activity.

In this paper, we focus on obtaining Hodgkin–Huxley (HH) type models for a few "prototypical" classes of neurons present in neocortex and thalamus. We restrict to the four most prominent cell classes, inspired from the classification of Connors and Gutnick (1990), which is augmented with one additional class. The 4 classes considered are the "fast spiking" (FS), "regular spiking" (RS), "intrinsically bursting" (IB) and in addition the "low-threshold spike" (LTS) cells. The latter class of neuron can also be used to model thalamic neurons, and the RS class is also used to model inhibitory cells with adaptation. This subdivision corresponds to classifying cells according to three qualitative criteria: (1) the presence or absence of spike-frequency adaptation; (2) the presence or absence of burst discharges from depolarizing stimuli; (3) the presence or absence of burst (or any other type of) discharge following hyperpolarizing inputs (rebound response).

To obtain HH models, we review, for each cell class, experimental data from different preparations, and derive HH models that capture the essential features of the intrinsic properties using a minimal number of voltage-dependent conductances. Our aim is double: (1) the models should capture the main intrinsic firing and response properties of excitatory and inhibitory neurons as displayed in the experiments; (2) if possible, the models should also be able to capture the diversity of intrinsic properties found across different cells and across different preparations.

Thus, a first goal of this paper is to provide an overview of these intrinsic properties and cell classes as seen experimentally in different preparations. A second goal is to provide models that capture these intrinsic properties and their diversity. Some of these models are fit to experimental data using automatic fitting procedures. Averaging parameters across fits obtained for different cells of the same class yields the most representative set of parameters for each class. The variance of these parameters also provides quantitative data about the cell-to-cell variability and diversity within a given cell class, which is an important piece of information presently not explicitly available in the literature.

2 Methods

All computational models were run under the NEURON simulation environment (Hines and Carnevale 1997). The equations of the models used throughout the papers are detailed first, and in the last section we describe the fitting methods.

2.1 Computational models

All models described here were single-compartment neurons (cylinder of diameter d and length L) described by the following membrane equation:

$$C_m \frac{\mathrm{d}V}{\mathrm{d}t} = -g_{\mathrm{leak}}(V - E_{\mathrm{leak}}) - I_{\mathrm{Na}} - I_{\mathrm{Kd}} - I_M - I_T - I_L, \tag{1}$$

where V is the membrane potential, $C_m = 1\ \mu\mathrm{F/cm}^2$ is the specific capacitance of the membrane, g_{leak} is the resting (leak) membrane conductance, E_{leak} is its reversal potential. These parameters are related to the input resistance R_{in}, which is normally measured experimentally. I_{Na} and I_{Kd} are the sodium and potassium currents responsible for action potentials, I_M is a slow voltage-dependent potassium current responsible for spike-frequency adaptation, I_L is a high-threshold calcium current and I_T is a low-threshold calcium current. These voltage-dependent currents are variants of the same generic equation:

$$I_j = \bar{g}_j\, m^M h^N\, (V - E_j), \tag{2}$$

where the current I_j is expressed as the product of respectively the maximal conductance, $\bar{g}_j$, activation (m) and inactivation variables (h), and the difference between the membrane potential V and the reversal potential E_j. The

gating of the channel is derived from the following first order kinetic scheme:

$$C \underset{\beta(V)}{\overset{\alpha(V)}{\rightleftharpoons}} O \tag{3}$$

where O and C are the open and closed states of the gate. The variables m and h represent the fraction of independent gates in the open state, following the convention introduced by Hodgkin and Huxley 1952. The steady-state activation and the time constant are, respectively, given by $m_\infty = \alpha/(\alpha+\beta)$ and $\tau_m = 1/(\alpha+\beta)$, and similarly for h.

2.2 Details for each voltage-dependent current

We detail below the kinetic parameters of the Hodgkin–Huxley type of models used in this paper. These models are taken from the literature and represent an arbitrary choice, as many other variants of these models were proposed. Parameter values for some of the models detailed below have been adjusted to voltage-clamp recordings in previous publications, and no attempt was made to find or estimate the kinetic parameters for the specific preparation used in this paper. All kinetics given below correspond to a temperature of 36°C.

2.2.1 Sodium and potassium currents to generate action potentials

The voltage-dependent Na^+ current was described by a modified version of Hodgkin–Huxley equations adapted for central neurons (Traub and Miles 1991), which is particularly well suited for hippocampal and cortical pyramidal cells:

$$\begin{aligned}
I_{\mathrm{Na}} &= \bar{g}_{\mathrm{Na}}\, m^3 h\, (V - E_{\mathrm{Na}}) \\
\frac{\mathrm{d}m}{\mathrm{d}t} &= \alpha_m(V)\,(1-m) \;-\; \beta_m(V)\, m \\
\frac{\mathrm{d}h}{\mathrm{d}t} &= \alpha_h(V)\,(1-h) \;-\; \beta_h(V)\, h \\
\alpha_m &= \frac{-0.32\,(V - V_T - 13)}{\exp[-(V - V_T - 13)/4] - 1} \\
\beta_m &= \frac{0.28\,(V - V_T - 40)}{\exp[(V - V_T - 40)/5] - 1} \\
\alpha_h &= 0.128\, \exp[-(V - V_T - 17)/18] \\
\beta_h &= \frac{4}{1 + \exp[-(V - V_T - 40)/5]}.
\end{aligned} \tag{4}$$

Unless stated otherwise, $\bar{g}_{\mathrm{Na}} = 50\,\mathrm{mS/cm^2}$ and $E_{\mathrm{Na}} = 50\,\mathrm{mV}$, the variable V_T adjusts spike threshold.

The "delayed-rectifier" K^+ current was described by Traub and Miles (1991):

$$\begin{aligned}
I_{\mathrm{Kd}} &= \bar{g}_{\mathrm{Kd}}\, n^4\, (V - E_K) \\
\frac{\mathrm{d}n}{\mathrm{d}t} &= \alpha_n(V)\,(1-n) \;-\; \beta_n(V)\, n \\
\alpha_n &= \frac{-0.032\,(V - V_T - 15)}{\exp[-(V - V_T - 15)/5] - 1} \\
\beta_n &= 0.5\, \exp[-(V - V_T - 10)/40],
\end{aligned}$$

where $\bar{g}_{\mathrm{Kd}} = 5\,\mathrm{mS/cm^2}$ and $E_K = -90\,\mathrm{mV}$, unless stated otherwise.

2.2.2 Slow potassium current for spike-frequency adaptation

A slow non-inactivating K^+ current was described by Yamada et al. (1989):

$$\begin{aligned}
I_M &= \bar{g}_M\, p\, (V - E_K) \\
\frac{\mathrm{d}p}{\mathrm{d}t} &= (p_\infty(V) - p)/\tau_p(V) \\
p_\infty(V) &= \frac{1}{1 + \exp[-(V + 35)/10]} \\
\tau_p(V) &= \frac{\tau_{\max}}{3.3\, \exp[(V + 35)/20] + \exp[-(V + 35)/20]},
\end{aligned}$$

where $\bar{g}_M$ was $0.004\,\mathrm{mS/cm^2}$ and $\tau_{\max} = 4\,\mathrm{s}$, unless stated otherwise.

2.2.3 Calcium currents to generate bursting

A first type of bursting was modeled by the high-threshold Ca^{2+} current, which was described by Reuveni et al. (1993):

$$\begin{aligned}
I_L &= \bar{g}_L\, q^2 r (V - E_{\mathrm{Ca}}) \\
\frac{\mathrm{d}q}{\mathrm{d}t} &= \alpha_q(V)\,(1-q) \;-\; \beta_q(V)\, q \\
\frac{\mathrm{d}r}{\mathrm{d}t} &= \alpha_r(V)\,(1-r) \;-\; \beta_r(V)\, r \\
\alpha_q &= \frac{0.055\,(-27 - V)}{\exp[(-27 - V)/3.8] - 1} \\
\beta_q &= 0.94\, \exp[(-75 - V)/17] \\
\alpha_r &= 0.000457\, \exp[(-13 - V)/50] \\
\beta_r &= \frac{0.0065}{exp[(-15 - V)/28] + 1},
\end{aligned}$$

where $\bar{g}_L$ is the maximum conductance of the I_L current, and the reversal potential for Ca^{2+} ions was $E_{\mathrm{Ca}} = 120\,\mathrm{mV}$.

A second type of bursting (rebound bursts) was modeled by the low-threshold Ca^{2+} current, which was initially designed for thalamic neurons (Destexhe et al. 1996a, b; see Huguenard and McCormick 1992 for voltage-clamp data),

and is given by:

$$I_T = \bar{g}_T\, s_\infty^2 u\, (V - E_{\mathrm{Ca}})$$
$$\frac{du}{dt} = (u_\infty(V) - u)/\tau_u(V)$$
$$s_\infty(V) = \frac{1}{1 + \exp[-(V + V_x + 57)/6.2]}$$
$$u_\infty(V) = \frac{1}{1 + \exp[(V + V_x + 81)/4]}$$
$$\tau_u(V) = \frac{30.8 + (211.4 + \exp[(V + V_x + 113.2)/5])}{3.7\,(1 + \exp[(V + V_x + 84)/3.2)]},$$

where $\bar{g}_T$ is the maximal conductance of the T-current and V_x is a uniform shift of the voltage dependence ($V_x = 2$ mV unless stated otherwise). Note that the activation variable s is considered here at steady-state, because the activation in fast compared to inactivation. This T-current model was also used with an independent activation variable (Destexhe et al. 1998; Fig. 10), but produced very similar results as the model with activation at steady-state (not shown).

2.3 Fitting methods

Some of the models (RS and FS cells) were adjusted to experimental data using automatic fitting procedures. The optimization of these models was done using a NEURON implementation of the simulated annealing method based on a simplex algorithm (Press et al. 1992). It is important to note that the optimization method described below does not fit the details of the V_m trajectory, such as the exact shape of the spike, the exact shape of the AHP, etc., but uses more qualitative criteria, such as the firing rate, the frequency-current relations, the adaptation time constant, the interspike intervals, the number of spikes in bursts, etc.

The strategy consists of a simplex (an assembly of $n + 1$ points, where n is the number of parameters) that moves in parameter space, where uphill steps are accepted with a certain probability depending on a slowly decreasing variable E (the 'temperature'). For very low temperature, the method becomes identical to the simplex algorithm, but during optimization it is less likely to get caught in local minima. A comparative survey showed (Vanier and Bower 1999), that for an intermediate number of parameters, the simulated annealing procedure was superior to other methods. We realized an automatic fitting of the models to recordings in rat somatosensory cortex in vitro. The error function consisted of a weighted sum over the absolute value of the differences in the time of the first spike after DC onset, the first, second and last interspike intervals, all values taken at three different DC levels:

$$e = \sum_i w_i \sqrt{(x_i^{\mathrm{data}} - x_i^{\mathrm{sim}})^2}. \qquad (5)$$

The index i labels the respective times and intervals of the responses obtained during stimulation at three different DC levels. This corresponds to a total of 12 quantities, which are fitted simultaneously to every cell. Since the data consisted of several trials, the reliability of these criteria could be estimated. In order to avoid that an (experimentally) unreliable feature strongly impacts on the error function, we chose the weights w_i to be the inverse of the SD of the experimental values. Large SDs thus lead to a reduced contribution to the error. However, in order to prevent an error that predominantly consists of the contribution of a very reliable feature, we introduced a cut-off: whenever the SD of a given feature was smaller than 3% of the mean experimental value, the weight was taken as the inverse of these 3%, rather than as the inverse of the SD itself.

The adjusted parameters were the leak conductance g_{leak} (bound by $g_{\mathrm{leak}}^{\mathrm{phys}}/3$ and $3 * g_{\mathrm{leak}}^{\mathrm{phys}}$, where $g_{\mathrm{leak}}^{\mathrm{phys}}$ is the leak conductance extracted from experiment), the maximal conductances $\bar{g}_{\mathrm{Na}}$ and $\bar{g}_{\mathrm{Kd}}$ of the sodium and potassium channels, a shift of their respective activation and inactivation curves V_T, as well as the maximal conductance of I_M and a factor τ_{max} scaling its time constant. The rationale for selecting which parameters were varied was to chose as few parameters as possible, but to allow a sufficient degree of flexibility of the models. Table 1 contains the complete list of the optimal parameters obtained for 13 RS-exc, 11 RS-inh and 14 FS cells. Those cells were all from rat somatosensory cortex.

Note that for other type of cells, such as bursting neurons, it was difficult to come up with a meaningful error function. Should the exact number of spikes in a burst matter? Should the exact timing (intra-burst ISI) be taken into account? Moreover, for those cell types, we did not have access to a large database, so it was not possible to evaluate how the error function would perform on different cells. For these reasons, the models for bursting (IB, LTS and thalamic) cells were hand-fitted. The problem of finding appropriate error functions should be addressed in a future study when sufficient data will be available.

2.4 Experimental methods

Experimental methods for intracellular recordings were given in previous papers, for the different preparations considered here: ferret primary visual cortex in vitro (Shu et al. 2003), rat somatosensory cortex in vitro (Toledo-Rodriguez et al. 2004), rat somatosensory thalamus in vitro (Huguenard and Prince 1992), cat primary visual cortex in vivo (Monier et al. 2003) and cat parietal cortex in vivo (Contreras and Steriade 1995). In addition, we also compared our models to published in vitro electrophysiological data from guinea-pig somatosensory cortex (McCormick et al. 1985) and frontal cortex

Table 1 Fitting results and parameters for all cells considered

	g_{leak} (nS)	$\bar{g}_{Na}$ (mS/cm^2)	$\bar{g}_{Kd}$ (mS/cm^2)	V_T (mV)	$\bar{g}_M$ (mS/cm^2)	τ_{max} (ms)	error
RS (exc.)	2.73	39	6.0	−59.72	0.20	1445.0	1.4
	2.43	56	6.0	−56.16	0.075	608.0	1.1
	1.33	60	5.1	−65.23	0.087	2269.0	2.8
	1.94	52	3.7	−55.43	0.15	653.5	0.6
	2.41	36	3.1	−62.86	0.088	1476.0	0.9
	1.43	50	6.0	−62.14	0.097	932.2	0.6
	1.42	60	5.5	−66.51	0.20	1340.0	1.7
	1.04	58	5.9	−62.87	0.10	959.0	0.8
	0.98	58	6.0	−59.54	0.082	1351.0	1.0
	0.91	45	2.0	−62.96	0.10	583.3	2.0
	2.23	59	3.1	−58.67	0.16	686.4	0.5
	2.54	42	3.9	−63.94	0.20	610.9	1.3
	3.34	30	6.0	−63.62	0.10	1691.0	1.5
MEAN	1.90	50	4.8	−61.5	0.13	1123.5	
SD	0.74	10	1.4	3.2	0.05	500.5	
RS (inh.)	3.06	40	5.7	−67.42	0.20	2928.0	1.1
	1.71	27	2.6	−61.89	0.038	1327.0	1.5
	0.96	36	5.5	−60.01	0.073	1996.0	1.2
	0.70	18	4.2	−74.67	0.17	1541.0	1.2
	5.69	14	5.2	−71.66	0.20	1490.0	1.6
	1.12	28	6.0	−66.54	0.09	2646.0	1.0
	1.83	40	3.3	−59.29	0.017	1594.0	5.4
	1.46	10	7.0	−62.51	0.035	1349.0	7.4
	2.19	40	2.9	−62.37	0.044	2997.0	3.0
	1.60	10	2.1	−67.85	0.098	934.4	1.6
MEAN	2.03	26.3	4.45	−65.4	0.097	1880.2	
SD	1.44	12.5	1.7	5.1	0.070	728.5	
FS (inh.)	12.35	31	7.0	−56.29	0.049	505.5	5.3
	10.00	32	6.0	−64.13	0.09	508.3	2.7
	14.81	38	5.2	−62.15	0.097	500.0	4.7
	29.06	51	5.7	−67.65	0.1	500.3	3.7
	12.68	60	4.5	−58.71	0.1	500.5	5.3
	5.84	40	5.4	−65.42	0.038	664.2	0.9
	3.86	58	6.6	−61.47	0.05	1056.0	0.3
	2.66	44	6.0	−58.20	0.1	503.9	1.4
	5.64	43	4.4	−63.44	0.1	505.7	1.4
	3.87	58	3.9	−57.94	0.079	501.9	1.5
	4.50	43	4.7	−63.85	0.05	1723.0	0.7
	0.46	60	3.9	−58.79	0.021	1454.0	0.7
	1.27	32	2.2	−67.17	0.071	596.6	1.2
	7.95	55	6.0	−60.49	0.039	2023.0	1.4
MEAN	8.21	46	5.1	−61.84	0.07	824.5	
SD	7.18	10	1.2	3.46	0.03	506.9	

For each cell (13 RS-exc, 10 RS-inh, 14 FS), the table indicates the parameters for the Hodgkin–Huxley type model that most optimally fit the data of that cell (see details in text; see Eq. 5 in Sect.2 for the definition of the error function). The same model was used to fit excitatory and inhibitory RS cells. The mean value and standard deviation (SD) of each fitted parameter are indicated for each cell type. All cells were from rat somatosensory cortex

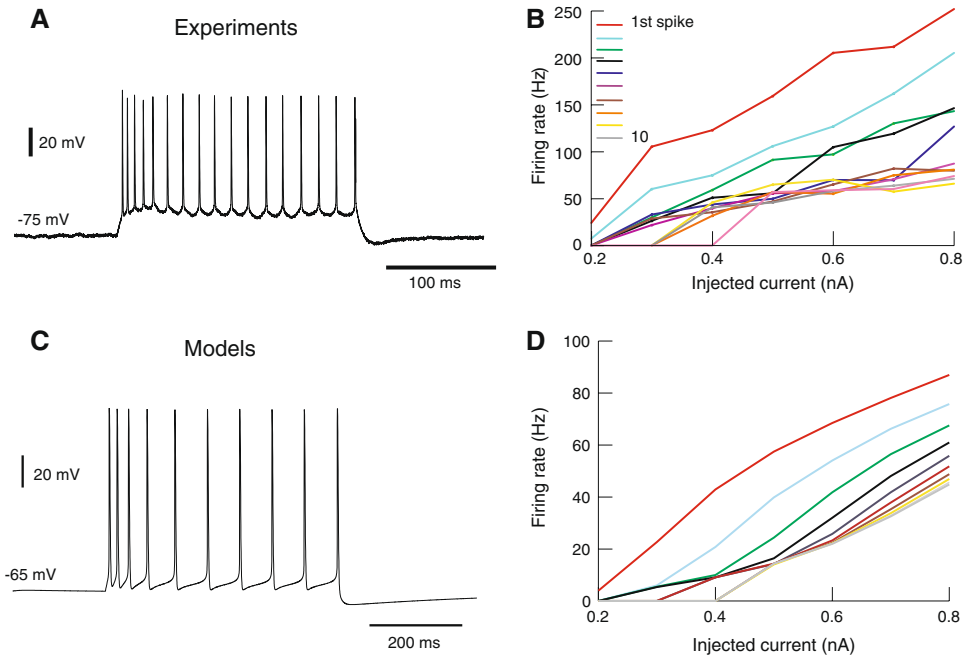

Fig. 1 Intracellular recordings of regular-spiking neurons in ferret visual cortex in vitro. **a** Responses to injection of a depolarizing current pulse (0.7 nA) showing the typical response of a regular spiking (RS) neuron, with spike-frequency adaptation. **b** Frequency–current (F/I) relation for this neuron. The instantaneous firing rate (inverse of the interspike interval) is represented as a function of the injected current (amplitude of the pulse). The *curves* indicated by different colors correspond to first, second, third,... spikes in the train. **c** Model of RS neuron, containing the currents I_{Na} and I_{Kd} responsible for spike generation, with an additional slow K^+ current (I_M) responsible for spike-frequency adaptation. These currents were simulated by Hodgkin–Huxley type models in NEURON. The model exhibited spike frequency adaptation following injection of depolarizing current pulses (*left* 0.5 nA injected). **d** Frequency–current (F/I) relation computed identically as for the experiments shown in **b**. Model parameters: $L = d = 96$ µm (0.29 nF capacitance), $g_{leak} = 1\times10^{-4}$ S/cm^2 (R_{in} of 34.5 MΩ), $E_{leak} = -70$ mV, $\bar{g}_{Na} = 0.05$ S/cm^2, $\bar{g}_{Kd} = 0.005$ S/cm^2, $\bar{g}_M = 7\times10^{-5}$ S/cm^2

(de la Peña and Geijo-Barrientos 1996). All cat, guinea-pig and ferret recordings used sharp electrodes, while the rat somatosensory system recordings used whole-cell patch electrodes.

3 Results

We successively consider below different cell classes, and show experiments and models for each cell class. Because very different preparations are used here (in vivo vs. in vitro, patch- vs. sharp-electrodes, different ages and species), we did not attempt to obtain a generic model for each class, but rather discuss the common features between different preparations, and integrate these features in the models.

3.1 Regular spiking neurons

By far the largest cell class in neocortex is the so-called "regular-spiking" (RS) neuron, which is in general excitatory and most often correlates with a spiny pyramidal-cell morphology. The typical response of RS cells to depolarizing current pulses are trains of spikes with adaptation, as illustrated here for a typical RS cell from ferret visual cortex in vitro (Fig. 1a). The instantaneous frequency-current relations obtained for successive interspike intervals, and for different current pulses is shown in Fig. 1b.

The simplest model of RS cells consists of conductances for generating spikes (I_{Na}, I_{Kd}; kinetics from Traub and Miles 1991), and in addition, a slow potassium current activated by depolarization, which we call here "I_M" (kinetics from Yamada et al. 1989). This model reproduces the typical firing characteristics of RS cells as recorded in ferret visual cortex in vitro (Fig. 1c) and their frequency–current relations (Fig. 1d). Note that the model reproduces the main features of spike-frequency adaptation, but the peak firing rate was different as the experiments. This is because the model had an input resistance typical of sharp-electrode recordings, and which was lower than the particular cell shown in Fig. 1a and b, and thus, displayed a lower peak firing rate for the same injected current.

The same model was also fit to RS cells from rat somatosensory cortex in vitro (Fig. 2). In this case, automatic fitting procedures were used to determine the optimal parameters (see Sect. 2). The results of the fitting are shown in Fig. 2 for two RS cells (one pyramidal cell in Fig. 2a, presumed

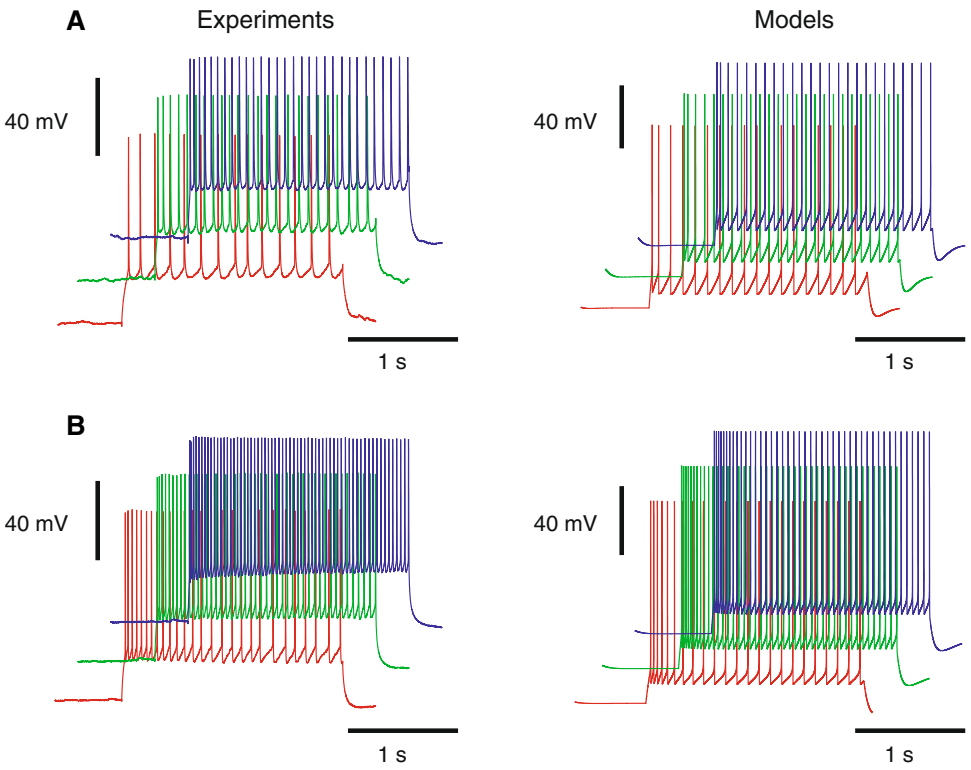

Fig. 2 Models of RS neurons based on somatosensory cortex in vitro. *Left panels* injection of depolarizing pulses in neurons from rat somatosensory cortex in vitro. *Right panels* same protocols simulated using the models. **a** Regular-spiking pyramidal neuron. Parameters: $L = d = 61.4\ \mu\text{m}$, $g_{\text{leak}} = 2.05 \times 10^{-5}\ \text{S/cm}^2$, $E_{\text{leak}} = -70.3\ \text{mV}$, $\bar{g}_{\text{Na}} = 0.056\ \text{S/cm}^2$, $V_T = -56.2\ \text{mV}$, $\bar{g}_{\text{Kd}} = 0.006\ \text{S/cm}^2$, $\bar{g}_M = 7.5 \times 10^{-5}\ \text{S/cm}^2$, $\tau_{\text{max}} = 608\ \text{ms}$. **b** Regular-spiking inhibitory neuron. Parameters: $L = d = 61.8\ \mu\text{m}$, $g_{\text{leak}} = 1.33 \times 10^{-5}\ \text{S/cm}^2$, $E_{\text{leak}} = -56.2\ \text{mV}$, $\bar{g}_{\text{Na}} = 0.01\ \text{S/cm}^2$, $V_T = -67.9\ \text{mV}$, $\bar{g}_{\text{Kd}} = 0.0021\ \text{S/cm}^2$, $\bar{g}_M = 9.8 \times 10^{-5}\ \text{S/cm}^2$, $\tau_{\text{max}} = 934\ \text{ms}$

excitatory, and one inhibitory interneuron in Fig. 2b). The complete list of the parameters obtained for 13 excitatory RS cells and 11 inhibitory RS cells from rat somatosensory cortex is shown in Table 1.

The fitting to different cells shows coherent values from cell to cell, but also a great disparity, depending on the parameter (Table 1). The coherent parameters are those concerning the V_m level and the spike generating mechanisms. The level of adaptation is more variable from cell to cell: the total conductance ($\bar{g}_M$) shows great variations, which can be partly attributed to the size of the recorded cell (compare with the g_{leak} values). However, the diversity of the decay time constants for adaptation, τ_{max}, cannot be explained by cell size. The values range from about 500 ms to more than 2 s (1123.5 ±500.5 s; see Table 1) and reflect cells with different rates of adaptation. The same observations also hold for inhibitory cells, as we will examine in more detail below.

3.2 Fast spiking neurons

Another major cell class in cerebral cortex is the "fast-spiking" (FS) neuron, which generally corresponds to aspiny inhibitory neurons. FS cells respond to depolarizing pulses by producing high-frequency trains of action potentials with little or no adaptation, as seen in ferret visual cortex in vitro (Fig. 3a). The frequency–current relations for successive spikes are almost superimposable (Fig. 3b). Similar firing behavior is also seen in FS neurons from rat somatosensory cortex in vitro (Fig. 4; note that some interneurons do show adaptation, as seen above in Fig. 2b). Many other intrinsic firing types have been described for cortical interneurons (Gupta et al. 2000), in addition to the classes outlined below.

FS cells are also the simplest type to model, as the conductances for generating spikes ($I_{\text{Na, Kd}}$) are sufficient. A model based on these two conductances reproduces well the intrinsic firing characteristics of FS cells of ferret visual cortex in vitro (Fig. 3c). The frequency-current relations are similar to experimental data (compare b to d in Fig. 3; note that in this model, as for the RS cell model, the input resistance and peak firing rate were not matched to experiments). In some cases, it is necessary to add an adaptation current (I_M) to account for the initial spike-frequency adaptation (Fig. 4). As for RS cells, we have used automatic fitting procedures to determine the optimal parameters for an ensemble of cortical FS cells recorded in rat somatosensory cortex in vitro. The results of this fit are shown in Fig. 4 for a fast spiking cell from rat somatosensory cortex. The model captured well the firing statistics of that particular neuron, although not the modulations of spike amplitude (the ionic origin of which is unknown). The full list of parameters obtained for 14 FS cells is given in Table 1.

3.3 Intrinsically bursting neurons

Another very common cell class is the "intrinsically bursting" (IB) neuron. This type of neuron generates bursts of action

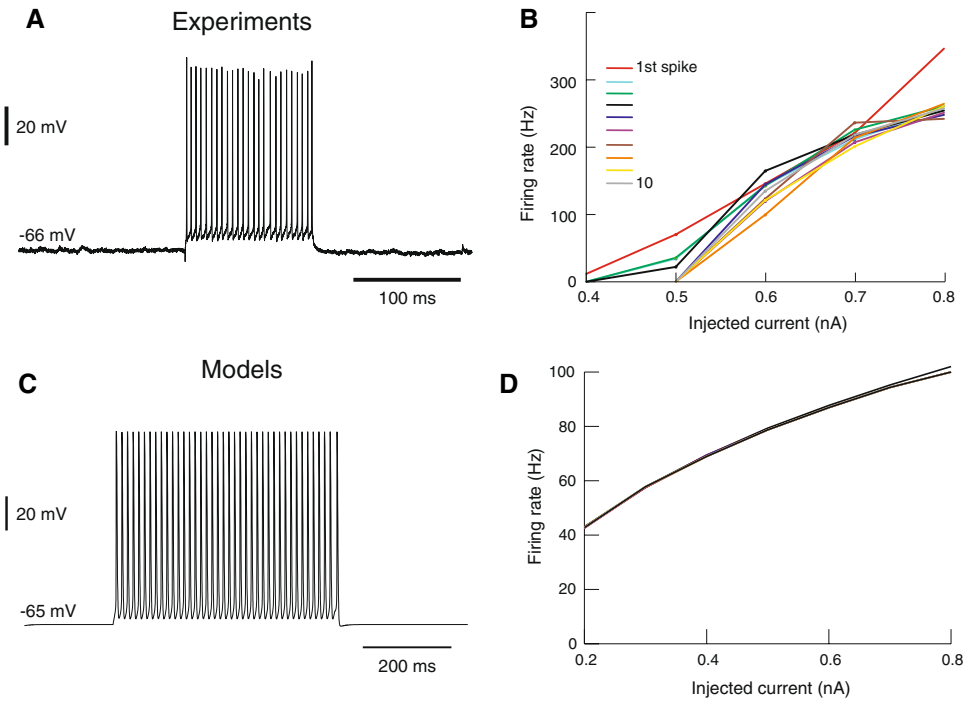

Fig. 3 "Fast spiking" neurons based on ferret visual cortex in vitro. **a** Response of a fast-spiking neuron to injection of a depolarizing current pulse (0.7 nA), showing negligible adaptation. **b** Frequency–current relation for this neuron, calculated identically as in Fig. 1b. **c** Response to depolarizing current in a model of fast spiking neuron. This model contained only I_{Na} and I_{Kd} simulated by Hodgkin–Huxley kinetics. **d** Frequency–current relation computed identically as for experiments in **b**. Model parameters were identical to RS cells (Fig. 1), except $L = d = 67$ µm (0.14 nF capacitance), $g_{leak} = 1.5\times10^{-4}$ S/cm^2 (R_{in} of 47 MΩ), $\bar{g}_{Kd} = 0.01$ S/cm^2 and no I_M

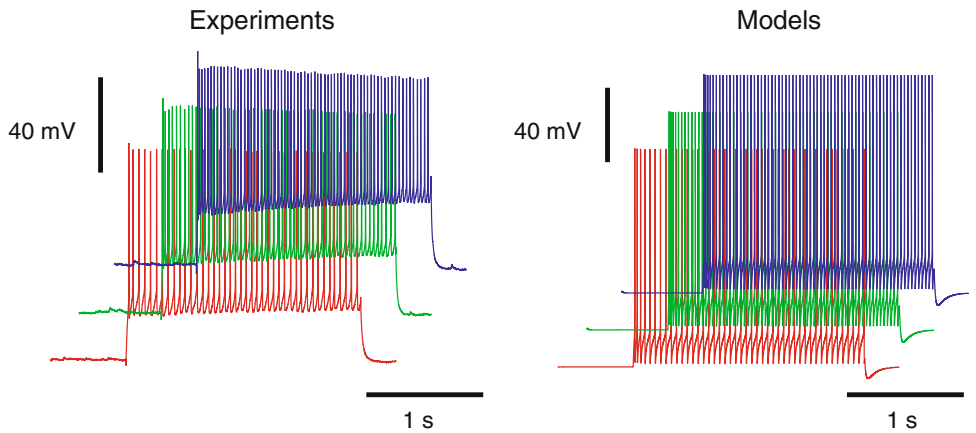

Fig. 4 Models of FS neurons based on somatosensory cortex in vitro. Left panels: injection of depolarizing pulses in a FS neuron from rat somatosensory cortex in vitro (steady-state frequencies, from bottom to top: 21, 29 and 34 Hz). *Right panels* same protocols simulated using the models (frequencies of 22, 31 and 34 Hz, respectively). Parameters: $L = d = 56.9$ µm, $g_{leak} = 3.8 \times 10^{-5}$ S/cm^2, $E_{leak} = -70.4$ mV, $\bar{g}_{Na} = 0.058$ S/cm^2, $V_T = -57.9$ mV, $\bar{g}_{Kd} = 0.0039$ S/cm^2, $\bar{g}_M = 7.87 \times 10^{-5}$ S/cm^2, $\tau_{max} = 502$ ms

potentials following depolarizing stimuli, and represents a few percent of the recorded cells in primary sensory cortex, both in vivo and in vitro. Figure 5a shows a bursting cell recorded in guinea pig somatosensory cortex in vitro (from McCormick et al. 1985) and Fig. 6a shows a bursting cell recorded in cat primary visual cortex in vivo. When submitted to depolarizing current pulses, IB cells first generate a burst of action potentials followed by single spikes with adaptation. This behavior is typical of IB neocortical neurons (Connors and Gutnick 1990).

We modeled IB cells based on a minimal set of voltage-dependent conductances. To generate the bursting behavior, we extended the previous model of RS cell by adding the L-type calcium current (kinetics from the model of Reuveni et al. 1993, based on experiments described in Sayer et al. 1990). In a first set of models, we generated IB type behavior by using moderate densities of I_L, and compared the behavior of the model with data obtained in the sensorimotor cortex of guinea pigs (Fig. 5a). This model generated an initial burst followed by an adapting train of action potentials (Fig. 5b,

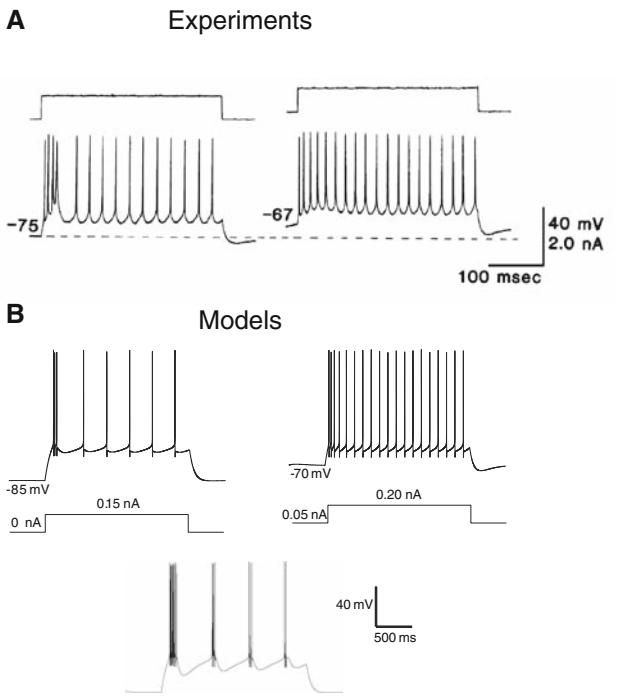

Fig. 5 Model of intrinsically bursting cell based on guinea-pig somatosensory cortex in vitro. The model consisted of a RS cell augmented with the L-type calcium current I_L, thus comprising I_{Na}, I_K, I_M and I_L currents. **a** Intrinsically bursting (IB) cell from guinea-pig somatosensory cortex in vitro (modified from McCormick et al. 1985). The response to the same depolarizing current pulse is shown at two different DC levels. **b** Response to depolarizing current in a model of IB cell. *Top panels* similar protocol as in **a**; *bottom panel* repetitive bursting activity with larger L-type conductance. Parameters: $L = d = 96\mu$m (0.29 nF capacitance), $g_{\mathrm{leak}} = 1 \times 10^{-5}$ S/cm^2, $E_{\mathrm{leak}} = -70$ mV, $\bar{g}_{\mathrm{Na}} = 0.05$ S/cm^2, $\bar{g}_{\mathrm{Kd}} = 0.005$ S/cm^2, $\bar{g}_M = 3 \times 10^{-5}$ S/cm^2, $\bar{g}_L = 0.0001$ S/cm^2 (0.0002 S/cm^2 for the *bottom panel*)

top). With larger L-type conductance, this model generated repetitive bursting activity (Fig. 5b, bottom). The latter behavior was similar to fast rhythmic bursting cells (Steriade et al. 1998) or chattering cells (Gray and McCormick 1996).

We also adjusted this model to data from cat primary visual cortex in vivo (Fig. 6a). The density of I_L was adjusted to match the response to depolarizing current pulses (Fig. 6b). As above, if depolarizing pulses were given from hyperpolarized levels, this model generated an initial burst followed by an adapting train of action potentials (Fig. 6b).

3.4 Low-threshold spiking neurons

In a previous study (Destexhe et al. 2001), we observed low-threshold spike (LTS) activity in a significant fraction (about 10%) of intracellularly recorded cells in cat association cortex in vivo (Fig. 7a). These LTS neurons generated adapting trains of action potentials in response to depolarizing current injection (Fig. 7a, left panel), similar to the classic "regular-spiking" response of cortical neurons. In addition, they generated a burst of action potentials in response to injection of hyperpolarizing current pulses (Fig. 7a, right panel). This property was also identified in deep layers of guinea-pig cerebral cortex in vitro (de la Peña and Geijo-Barrientos 1996; see Fig. 7b) and was shown to be due to the presence of the T-type (low-threshold) calcium current I_T.

We have attempted to model these intrinsic firing properties based on a minimal set of voltage-dependent conductances. To generate rebound bursting behavior, the T-type calcium current was included (kinetics from Destexhe et al. 1996a, b) and its peak amplitude was adjusted to match voltage-clamp recordings of this current in pyramidal neurons (de la Peña and Geijo-Barrientos 1996). A density of T-channels of 0.8 mS/cm^2 was needed to match the relatively small amplitude of this current measured in pyramidal neurons. Using this density, the model could generate weak rebound spikes at the offset of hyperpolarizing current (Fig. 8a, -60 mV). To generate the classic "regular-spiking" behavior (Fig. 8b, -70 mV), the model included three voltage-dependent currents identical to the RS cells described above: a slow voltage-dependent K^+ current (I_M), as well as I_{Na} and I_{Kd} currents for action potential generation. When depolarizing pulses were given from hyperpolarized levels, this model generated an initial burst followed by an adapting train of action potentials (Fig. 8c, -80 mV), which is a feature often observed in neocortical neurons (Connors and Gutnick 1990).

In addition, we also considered LTS cells from rat somatosensory cortex in vitro (Fig. 9, *Experiments*). As seen above, this LTS cell generated adapting trains of action potentials in response to depolarizing pulses (Fig. 9a, *Experiments*), as well as rebound burst activity at the offset of hyperpolarizing current pulses (Fig. 9b, *Experiments*). We used the same model as above, but changed the parameters such that it matches the input resistance of this LTS neuron (which was 210 MΩ for this particular cell), and approximates at best the frequency/current relationship of the cell (not shown). The resulting model is shown in Fig. 9a and b (*Models*) for the exact same protocol as for the experiments. Interestingly, one sees that the model can generate an initial burst in depolarizing responses, in a manner similar to some of the model traces of IB cells shown in Fig. 5b. The two types of calcium current seem to have a similar effect for this initial burst response.

3.5 Thalamic relay neurons

It is important to note that the model of LTS cell is very similar to models for thalamic relay cells. There are, however, two notable differences. First, thalamic relay cells do not show spike-frequency adaptation, so no adaptation current, such as I_M, is needed. Second, the thalamic relay cell produces more powerful bursts compared to cortical LTS cells,

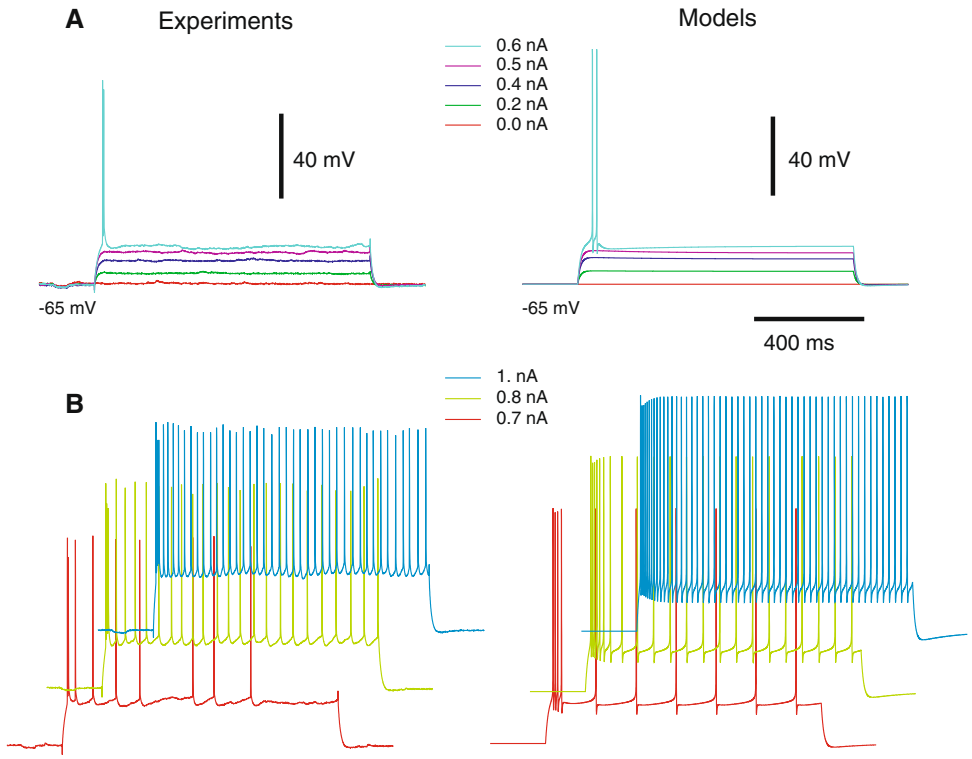

Fig. 6 Model of intrinsically bursting cell based on cat visual cortex neurons in vivo. *Left* intracellular recording of an intrinsically bursting (IB) cell from cat primary visual cortex in vivo. *Right* model consisting of a RS cell augmented with the L-type calcium current I_L, thus comprising I_{Na}, I_K, I_M and I_L currents. **a** Responses to depolarizing current pulses from 0 to 0.6 nA, as indicated. Note that for 0.6 nA, both data and model generated a doublet of spike. **b** Responses to current pulses from 0.7 to 1 nA, for which repetitive firing was evoked. Model parameters: $L = d = 96\mu m$ (0.29 nF capacitance), $g_{leak} = 1 \times 10^{-4}$ S/cm^2 (R_{in} of 34.5 MΩ), $E_{leak} = -75$ mV, $\bar{g}_{Na} = 0.05$ S/cm^2, $V_T = -58$ mV, $\bar{g}_{Kd} = 0.0042$ S/cm^2, $\bar{g}_M = 4.2 \times 10^{-5}$ S/cm^2, $\tau_{max} = 1,000$ ms, $\bar{g}_L = 0.00012$ S/cm^2

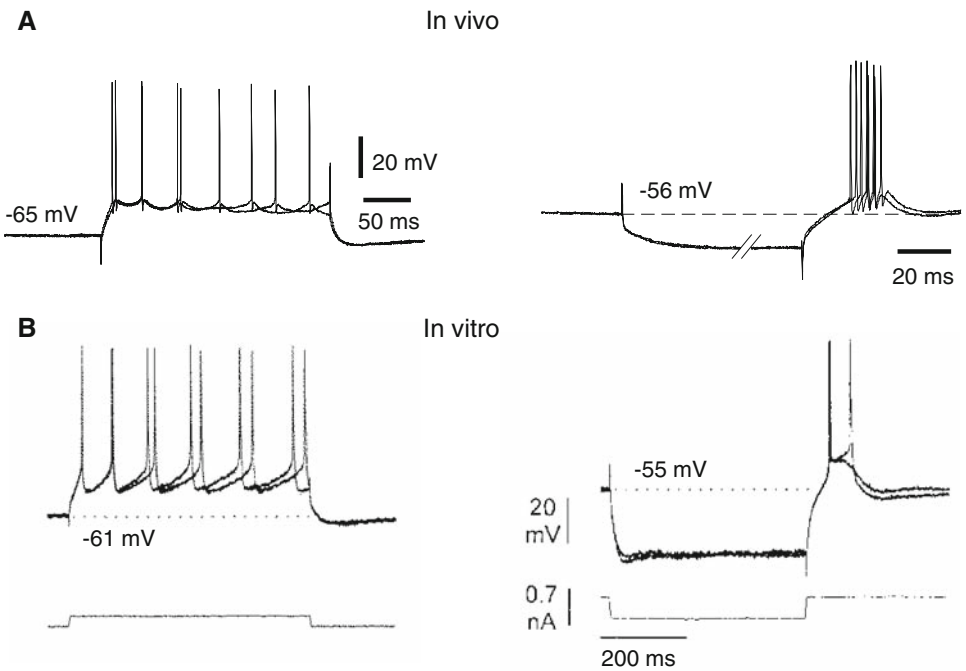

Fig. 7 Rebound bursting properties of cortical pyramidal cells in vivo and in vitro. **a** Rebound bursting cell from cat parietal cortex in vivo (from Destexhe et al. 2001). **b** Rebound bursting cell from guinea-pig frontal cortex in vitro (adapted from de la Peña and Geijo-Barrientos 1996). In both cases, the response to depolarizing current pulses (*left*) was similar to a regular spiking cell. In addition, LTS cells produce a burst of action potentials upon release from inhibition or in response to hyperpolarizing current pulses as shown here (*right* −0.1 nA pulse of 200 ms in **a**, truncated for clarity)

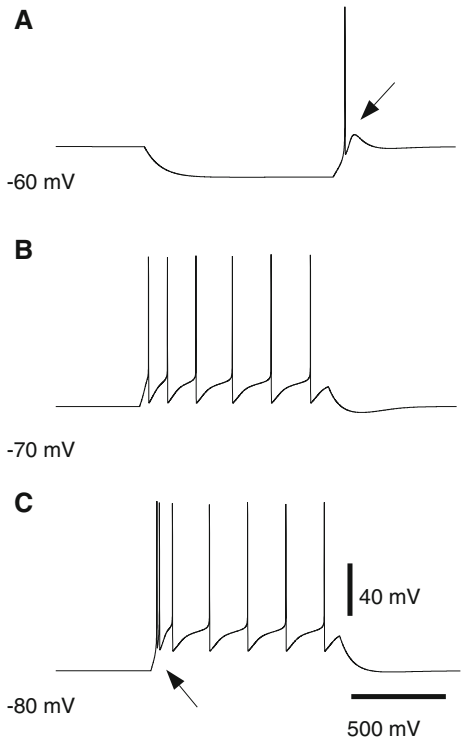

Fig. 8 Model of rebound bursting cell of cat association cortex in vivo. The model consisted of a RS cell augmented with the T-type calcium current I_T, thus comprising I_{Na}, I_K, I_M and I_T currents. **a** Rebound response at the offset of a hyperpolarizing current pulse (−0.1 nA). **b** Adapting train of action potentials with depolarizing current pulses. **c** Similar depolarizing pulse showing a burst of action potentials followed by single spikes. *Arrows* indicate the rebound response mediated by I_T (one action potential in **a**, two action potentials in **c**). Model parameters: $L = d = 96\mu m$ (0.29 nF capacitance), $g_{leak} = 1 \times 10^{-5}$ S/cm^2, $E_{leak} = -85$ mV, $\bar{g}_{Na} = 0.05$ S/cm^2, $\bar{g}_{Kd} = 0.005$ S/cm^2, $\bar{g}_M = 3 \times 10^{-5}$ S/cm^2, $\bar{g}_T = 0.0004$ S/cm^2. Figure modified from Destexhe et al. 2001

presumably because the T-type calcium current I_T has a larger conductance in thalamic cells. In voltage-clamp experiments, the peak amplitude of I_T in pyramidal neurons of guinea-pig cerebral cortex is of about 0.4–0.8 nA (de la Peña and Geijo-Barrientos 1996), which is small compared to the peak amplitude of I_T in thalamic relay cells (5.8 ± 1.7 nA in Destexhe et al. 1998). Figure 10 shows models of thalamic relay cell obtained previously. Current-clamp (Fig. 10a) and voltage-clamp (Fig. 10c) recordings were used to adjust the model. A detailed model based on morphological reconstructions was first obtained (Fig. 10b). This model was then simplified into a single-compartment model comprising I_T, I_{Na} and I_{Kd} currents (Fig. 10d; same kinetics as above; see details in Destexhe et al. 1998).

Discussion

In this paper, we have provided an overview of simplified models for the most frequent electrophysiological classes of neurons in cortex and thalamus. The models presented are not new, and exist in the literature for most of them, but their parameters were adjusted to experimental data from different preparations, to obtain a series of models for each cell class, and using a consistent model format. More specifically, the original contributions of the paper are: (1) to provide a set of models fit to different neuron classes (RS, FS, LTS, Thalamic) in the same preparation (rat somatosensory cortex and thalamus in vitro); (2) to provide examples of the same models fit to other preparations, including guinea-pigs and cats in vivo; (3) to provide an automatic fitting for several cells of the same class (see Table 1), which allows one to directly estimate the cell-to-cell variability within a given cell class. None of these data are available in the literature, and we believe this information should be useful to build thalamocortical networks where not only the different classes of intrinsic properties are present, but also the cell-to-cell variability within each class.

The models considered here are the simplest types of biophysical models where the intrinsic properties arise from voltage-dependent conductances, each described by differential equations (Hodgkin–Huxley type models). Simplified single-compartment HH type models were proposed for thalamic cells and derived from more complex models (Destexhe et al. 1996a, b, 1998), and a similar approach of reduction to a single-compartment model was proposed for cortical neurons (Stratford et al. 1989; Destexhe et al. 2001). Simplified models for bursting cells were also studied since many years (Rinzel 1987; Rose and Hindmarsh 1989; Rinzel and Ermentrout 1989). More recently, a two-dimensional integrate and fire model was proposed to account for a broad range of intrinsic firing properties (Izhikevich 2004; Brette and Gerstner 2005). The present work to obtain simplified models for different cell classes, using data from different cells and different preparations, complements these previous modeling efforts.

It is important to note that the models proposed here are not uniquely suitable to represent these classes of neurons. As outlined above, other models exists for the different ionic currents considered here, and we did not attempt to obtain the kinetic parameters from voltage-clamp data in the different preparations. In addition, some of the behaviors can be modeled using different types of ion channels, such as adaptation which can be modeled from calcium-dependent conductances. The present study shows that minimal models can capture the main electrophysiological features of several classes of neurons based on only five voltage-dependent currents. Such models can be used in network simulations where realistic intrinsic properties are needed. Such models are implementable on specific analog microcircuits (ASIC), and some of these models (the RS and FS cells of Figs. 1, 3) have already been implemented (Renaud et al. 2007; Zou et al. 2006). Since different cell types can be modeled using

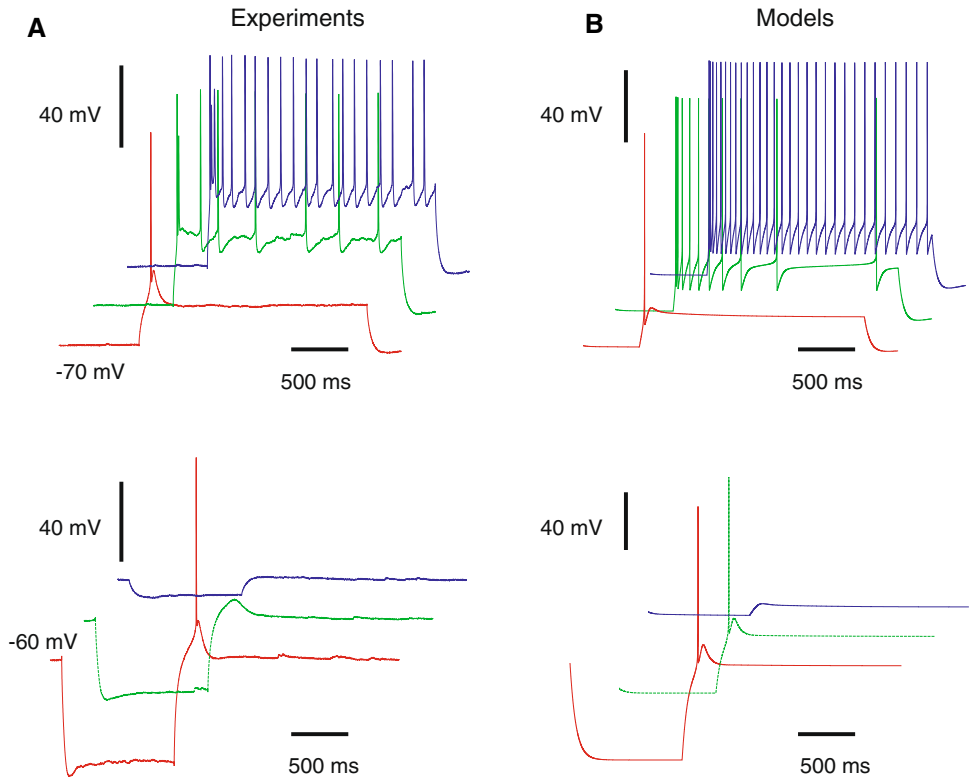

Fig. 9 Model of rebound bursting cell based on rat somatosensory cortex in vitro. The model had the same current as the "cat" model, but with different parameters. **a** LTS cell from rat somatosensory cortex in vitro. The top panel shows the response to depolarizing current pulses, while the response to hyperpolarizing pulses is shown in the bottom panel. Values of the injected current were: −0.015, 0.067 and 0.13 nA for depolarizing pulses (DC current was −0.11 nA to bring the cell to −70 mV; they were of −0.36, −0.24 and −0.09 nA for hyperpolarizing pulses (pre-pulse current of −0.056 nA to bring the cell to −60 mV. **b** Same protocols simulated using the model. The parameters were: $L = d = 89.2\mu$m (0.25 nF capacitance), $g_{\text{leak}} = 1.9 \times 10^{-5}$ S/cm^2, $E_{\text{leak}} = -50$ mV, $\bar{g}_{\text{Na}} = 0.05$ S/cm^2, $V_T = -50$ mV, $\bar{g}_{\text{Kd}} = 0.004$ S/cm^2, $\bar{g}_M = 2.8 \times 10^{-5}$ S/cm^2, $\bar{g}_T = 0.0004$ S/cm^2, $V_x = -7$ mV

5 or less generic conductances, it should be feasible to design a single chip with 5 voltage-dependent conductances but tunable parameters, so that the same chip could be used for all the major cell types in network simulations (work in progress with S. Renaud and colleagues within the FACETS European project).

A few important additional points must be noted. First, the choice of a specific cell class is not restricted to excitatory or inhibitory neurons. Any cell class can be used for any cell type, for instance LTS and RS type of intrinsic properties have been found for both excitatory or inhibitory neurons in cortex (Gupta et al. 2000). In addition, the LTS cell class can be used to model thalamic neurons.

Second, we described here four distinct cell properties, but in general the properties are not so clear-cut. It is important to note that these models can be changed at will to diversify the neuron types. For example, the time constant $\tau_{\max}$ of the adaptation current I_M can be adjusted to yield fast or slow adaptation. From our fitting to spike-frequency adaptation, the values of $\tau_{\max}$ range from a few hundred milliseconds to several seconds (see Table 1).

A third point to emphasize is that the automatic fitting realized here for RS and FS cells shows an unexpectedly high diversity from cell to cell, even within the same cell class (see Table 1). For example, the rate of spike frequency adaptation shows a considerable cell-to-cell variability. We did not have the data to perform a similar study on the other cell types, IB, LTS and thalamic cells. All these other cell types are bursting, and it is difficult to design a meaningful error function to appropriately quantify bursts (see Tien and Guckenheimer 2008). Such error functions should be tested on a database of several neurons for each class of bursting cell, which should be done when these data will be available.

Finally, it is important to note that another possible approach to design simple representations of cellular models is based on the integrate-and-fire model. For instance, the integrate-and-fire-or-burst (Smith et al. 2000) or the Izhikevich (2004) type of models are two-variable extensions of the integrate-and-fire model that can capture some of the diversity of firing patterns in cortical neurons (Izhikevich 2004). Another variant is the adaptive exponential integrate-and-fire model (Brette and Gerstner 2005), which displays

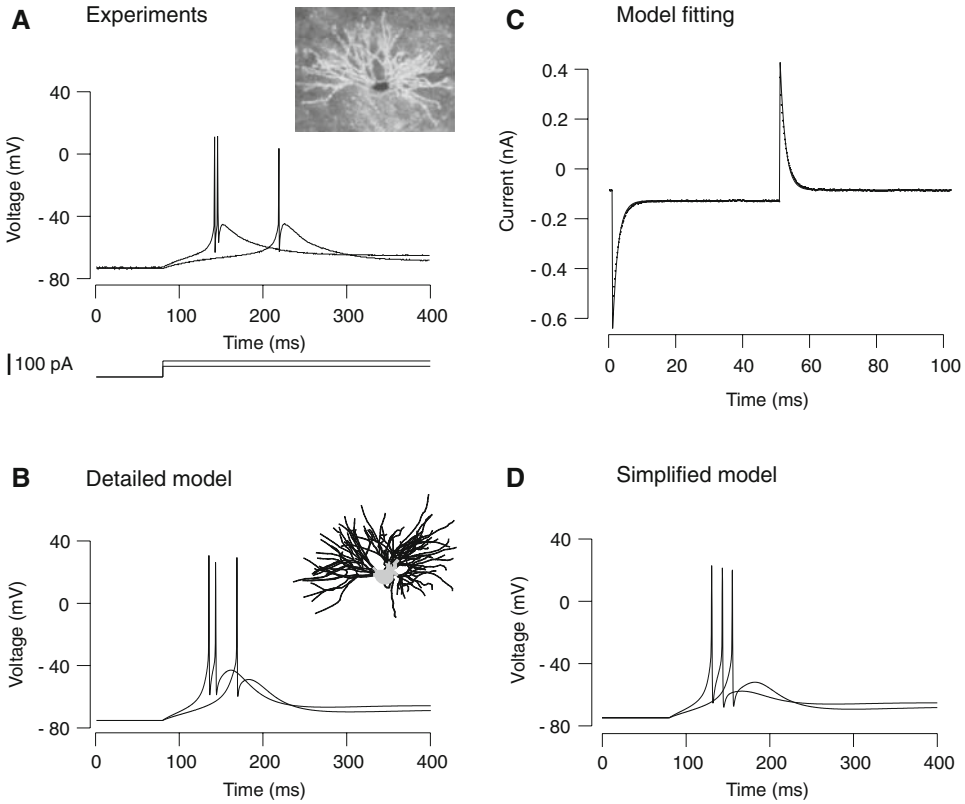

Fig. 10 Model of thalamic relay neuron from rat somatosensory thalamus in vitro. **a** Current-clamp recordings of a relay cell from the ventrobasal thalamus (inset), subjected to depolarizing current pulses from the resting membrane potential. The cell produced a rebound burst of action potentials. **b** Detailed model based on the morphology of the recorded cell (which was reconstructed and incorporated into simulations). The inset shows the reconstructed cell model (soma in *gray*). **c** Adjustment of a one-compartment model to passive responses recorded in voltage-clamp in the cell shown in **a** (*dots*; model showed as a continuous trace). **d** Current-clamp simulation of the same protocol as in **a** using the simplified model. Modified from Destexhe et al. 1998 where all details were given

a more realistic subthreshold behavior. The latter model is also easy to fit to experimental data and therefore should also provide a good match to intracellular recordings. It is also implementable on analog microcircuits (ongoing work of K. Meier and colleagues at Heidelberg University, within the *FACETS* European project).

In conclusion, we have presented here simple Hodgkin–Huxley type models for the main cell classes of cortical and thalamic neurons, using at most 5 conductances. This type of model is more complex than nonlinear integrate-and-fire models (Smith et al. 2000; Izhikevich 2004; Brette and Gerstner 2005), but is also more realistic because the ionic currents are identified and can be fit to physiological measurements such as voltage-clamp data if needed. It is also simpler than detailed models that incorporate the cellular morphology such as dendrites and axon, and which would include conductance kinetics directly estimated from the same preparation (e.g., Destexhe et al. 1998). Simple Hodgkin–Huxley models are well suited for building network simulations in which the effect of neuromodulators or pharmacological agents on identified conductances can be tested. Finally, it is possible that specific network properties arise from the nonlinear interaction between intrinsic and synaptic conductances, in which case it would be necessary to model intrinsic properties by conductances (which is not the case in simplified models such as Izhikevich 2004 or Brette and Gerstner 2005). Thus, the types of Hodgkin–Huxley model considered here represent one of the many possible compromises between simplicity and biological realism.

Acknowledgments Research supported by the CNRS, ANR, ACI, HFSP and the European Community (FACETS grant FP6 15879). We would like to thank Andrew P. Davison for the NEURON implementation of the fitting algorithm.

References

Achard P, De Schutter E (2006) Complex parameter landscape for a complex neuron model. PLoS Comput Biol 2:e94

Baldi P, Vanier MC, Bower JM (1998) On the use of Bayesian methods for evaluating compartmental neural models. J Comput Neurosci 5:285–314

Bhalla US, Bower JM (1993) Exploring parameter space in detailed single neuron models: simulations of the mitral and granule cells of the olfactory bulb. J Neurophysiol 69:1948–1965

Brette R, Gerstner W (2005) Adaptive exponential integrate-and-fire model as an effective description of neuronal activity. J Neurophysiol 94:3637–3642

Cauller LJ, Connors BW (1992) Functions of very distal dendrites: experimental and computational studies of Layer I synapses on neocortical pyramidal cells. In: McKenna T, Davis J, Zornetzer SF (eds) Single neuron computation, Academic Press, Boston

Connors BW, Gutnick MJ (1990) Intrinsic firing patterns of diverse neocortical neurons. Trends Neurosci 13:99–104

Contreras D, Steriade M (1995) Cellular basis of EEG slow rhythms: a study of dynamic corticothalamic relationships. J Neurosci 15:604–622

de la Peña E, Geijo-Barrientos E (1996) Laminar organization, morphology and physiological properties of pyramidal neurons that have the low-threshold calcium current in the guinea-pig frontal cortex. J Neurosci 16:5301–5311

Destexhe A (2001) Simplified models of neocortical pyramidal cells preserving somatodendritic voltage attenuation. Neurocomputing 38:167–173

Destexhe A, Bal T, McCormick DA, Sejnowski TJ (1996) Ionic mechanisms underlying synchronized oscillations and propagating waves in a model of ferret thalamic slices. J Neurophysiol 76:2049–2070

Destexhe A, Contreras D, Steriade M, Sejnowski TJ, Huguenard JR (1996) In vivo, in vitro and computational analysis of dendritic calcium currents in thalamic reticular neurons. J Neurosci 16: 169–185

Destexhe A, Neubig M, Ulrich D, Huguenard JR (1998) Dendritic low-threshold calcium currents in thalamic relay cells. J Neurosci 18:3574–3588

Destexhe A, Contreras D, Steriade M (2001) LTS cells in cerebral cortex and their role in generating spike-and-wave oscillations. Neurocomputing 38:555–563

Druckmann S, Banitt Y, Gidon A, Schurmann F, Markram H, Segev I (2007) A novel multiple objective optimization framework for constraining conductance-based neuron models by experimental data. Front Neurosci 1:7–18

Eichler-West R, Wilcox G (1997) Robust parameter selection for compartmental models of neurons using evolutionary algorithms. In: Bower JM (ed) Computational neuroscience: trends in research 1997. Plenum Press, New York, pp 75–80

Foster WR, Ungar LH, Schwaber JS (1993) Significance of conductances in Hodgkin–Huxley models. J Neurophysiol 70:2502–2518

Golowasch J, Goldman MS, Abbott LF, Marder E (2002) Failure of averaging in the construction of a conductance-based neuron model. J Neurophysiol 87:1129–1131

Gray CM, McCormick DA (1996) Chattering cells: superficial pyramidal neurons contributing to the generation of synchronous oscillations in the visual cortex. Science 274:109–113

Gupta A, Wang Y, Markram H (2000) Organizing principles for a diversity of GABAergic interneurons and synapses in the neocortex. Science 287:273–278

Haufler D, Morinc F, Lacaille JC, Skinner FK (2007) Parameter estimation in single-compartment neuron models using a synchronization-based method. Neurocomputing 70:1605–1610

Hines ML, Carnevale NT (1997) The neuron simulation environment. Neural Comput 9:1179–1209

Hodgkin AL, Huxley AF (1952) A quantitative description of membrane current and its application to conduction and excitation in nerve. J Physiol 117:500–544

Holmes W, Ambros-Ingerson J, Grover L (2006) Fitting experimental data to models that use morphological data from public databases. J Computat Neurosci 20:349–365

Huguenard JR, McCormick DA (1992) Simulation of the currents involved in rhythmic oscillations in thalamic relay neurons. J Neurophysiol 68:1373–1383

Huguenard JR, Prince DA (1992) A novel T-type current underlies prolonged Ca^{2+}-dependent bursts firing in GABAergic neurons of rat thalamic reticular nucleus. J Neurosci 12:3804–3817

Izhikevich EM (2004) Which model to use for cortical spiking neurons? IEEE Trans Neural Netw 15:1063–1070

Jolivet R, Lewis TJ, Gerstner W (2004) Generalized integrate-and-fire models of neuronal activity approximate spike trains of a detailed model to a high degree of accuracy. J Neurophysiol 92:959–976

LeMasson G, Maex R (2001) Introduction to equation solving and parameter fitting. In: De Schutter E (ed) Computational neuroscience: realistic modeling for experimentalists. CRC Press, Boca Raton, pp 1–22

Llinás RR (1988) The intrinsic electrophysiological properties of mammalian neurons: a new insight into CNS function. Science 242:1654–1664

Major G, Larkmann AU, Jonas P, Sakmann B, Jack JJB (1994) Detailed passive cable models of whole-cell recorded CA3 pyramidal neurons in rat hippocampal slices. J Neurosci 14:4613–4638

Marder E, Tobin AE, Grashow R (2007) How tightly tuned are network parameters? Insight from computational and experimental studies in small rhythmic motor networks. Prog Brain Res 165: 193–200

McCormick DA, Connors BW, Lighthall JW, Prince DA (1985) Comparative electrophysiology of pyramidal and sparsely spiny stellate neurons of the neocortex. J Neurophysiol 54:782–806

Monier C, Chavane F, Baudot P, Graham LJ, Frégnac Y (2003) Orientation and direction selectivity of synaptic inputs in visual cortical neurons: a diversity of combinations produces spike tuning. Neuron 37:663–680

Press WH, Flannery BP, Teukolsky SA (1992) Numerical recipes in C: The Art of Scientific Computing, 2nd edn. Cambridge University Press, Cambridge

Rall W, Burke RE, Holmes WR, Jack JJ, Redman SJ, Segev I (1992) Matching dendritic neuron models to experimental data. Physiol Rev 72:S159–S186

Rapp M, Segev I, Yarom Y (1994) Physiology, morphology and detailed passive models of guinea-pig cerebellar Purkinje cells. J Physiol 474:101–118

Rauch A, La Camera G, Lüscher H-R, Senn W, Fusi S (2003) Neocortical pyramidal cells respond as integrate-and-fire neurons to in vivo like input currents. J Neurophysiol 90:1598–1612

Renaud S, Tomas J, Bornat Y, Daouzli A, Saïghi S (2007) Neuromimetic ICs with analog cores: an alternative for simulating spiking neural networks. In: International symposium on circuits and systems (ISCAS07), New-Orleans, USA, 27–30 May (ISBN 1-4244-0921-1), pp 3355–3358

Reuveni I, Friedman A, Amitai Y, Gutnick MJ (1993) Stepwise repolarization from Ca^{2+} plateaus in neocortical pyramidal cells: evidence for nonhomogeneous distribution of HVA Ca^{2+} channels in dendrites. J Neurosci 13:4609–4621

Rinzel J (1987) A formal classification of bursting mechanisms in excitable systems. In: Teramoto E, Yamaguti M (eds) Mathematical topics in population biology, morphogenesis and neurosciences. Springer, Berlin, pp 267–281

Rinzel J, Ermentrout GB (1989) Analysis of neural excitability and oscillations. In: Koch C, Segev I (eds) Methods in neuronal modeling. MIT press, Cambridge, pp 135–169

Rose RM, Hindmarsh JL (1989) The assembly of ionic currents in a thalamic neuron. I. The three-dimensional model. Proc R Soc Lond B Biol Sci 237:267–288

Sayer RJ, Schwindt PC, Crill WE (1990) High- and low-threshold calcium currents in neurons acutely isolated from rat sensorimotor cortex. Neurosci Lett 120:175–178

Shu Y, Hasenstaub A, Badoual M, Bal T, McCormick DA (2003) Barrages of synaptic activity control the gain and sensitivity of cortical neurons. J Neurosci 23:10388–10401

Smith GD, Cox CL, Sherman M, Rinzel J (2000) Fourier analysis of sinusoidally driven thalamocortical relay neurons and a minimal integrate-and-fire-or-burst model. J Neurophysiol 83:588–610

Steriade M, Timofeev I, Durmüller N, Grenier F (1998) Dynamic properties of corticothalamic neurons and local cortical interneurons generating fast rhythmic (30–40 Hz) spike bursts. J Neurophysiol 79:483–490

Stratford K, Mason A, Larkman A, Major G, Jack J (1989) The modeling of pyramidal neurones in the visual cortex. In: Durbin A, Miall C, Mitchison G (eds) The computing neuron. Addison-Wesley, Workingham, pp 296–321

Stuart G, Spruston N (1998) Determinants of voltage attenuation in neocortical pyramidal neuron dendrites. J Neurosci 18:3501–3510

Tawfik B, Durand DM (1994) Nonlinear parameter-estimation by linear associationapplication to a 5-parameter passive neuron model. IEEE Trans Biomed Eng 41:461–469

Taylor AL, Hickey TJ, Prinz AA, Marder E (2006) Structure and visualization of high-dimensional conductance spaces. J Neurophysiol 96:891–905

Tien JH, Guckenheimer J (2008) Parameter estimation for bursting neural models. J Computat Neurosci 24:358–373

Toledo-Rodriguez M, Blumenfeld B, Wu C, Luo J, Attali B, Goodman P, Markram H (2004) Correlation maps allow neuronal electrical properties to be predicted from single-cell gene expression profiles in rat neocortex. Cereb Cortex 14:1310–1327

Traub RD, Miles R (1991) Neuronal networks of the Hippocampus. Cambridge University Press, Cambridge

Vanier MC, Bower JM (1999) A comparative survey of automated parameter-search methods for compartmental neural models. J Comput Neurosci 7:149–171

Yamada WM, Koch C, Adams PR (1989) Multiple channels and calcium dynamics. In: Koch C, Segev I (eds) Methods in neuronal modeling. MIT press, Cambridge, pp 97–134

Zou Q, Bornat Y, Saïghi S, Tomas J, Renaud S, Destexhe A (2006) Analog-digital simulations of full conductance-based networks of spiking neurons with spike timing dependent plasticity. Network 17:211–233